Graz University of Technology
Institute of Applied Mechanics

Preprint Series

Preprint No 01/2013

Time Domain Boundary Element Formulation for Partially Saturated Poroelasticity

Peng Li, Martin Schanz
Institute of Applied Mechanics, Graz University of Technology

Published in *Engineering Analysis with Boundary Elements*,
37(11), 1483–1498, 2013
DOI: 10.1016/j.enganabound.2013.08.002
Latest revision: June 25, 2013

Abstract

Based on the Mixture theory and the principles of continuum mechanics, a dynamic three–phase model for partially saturated poroelasticity is established as well as the corresponding governing equations in Laplace domain. The three-dimensional fundamental solutions are deduced following Hörmander's method. Based on the weighted residual method, the boundary integral equations are established. The boundary element formulation in time domain for partial saturated media is obtained after regularization by partial integration, spatial discretization, and the time discretization with the Convolution Quadrature Method. The proposed formulation is validated with the semi-analytical one-dimensional solution of a column. Studies with respect to the spatial and temporal discretisation show its sensitivity on a fine enough mesh. An half-space example allows to study the wave fronts. Finally, the proposed formulation is used to compute the vibration isolation of an open trench.

1 Introduction

Elastic wave propagation in porous media is of great importance in many areas as acoustics, geomechanics, biomechanics, petroleum engineering, geophysics, materials science, etc. In geotechnical engineering, the porous media are mainly soils and rocks. The analysis of such geomaterials under dynamic loadings is of interest for various applications in the field of geotechnical engineering as pile driving, dynamic compaction, vibratory isolation, earthquake engineering, etc.

Under natural conditions there are no absolutely saturated or dry geomaterials, instead the material is partial saturated. Such kind of materials have three phases, i.e., the solid phase is coupled with the liquid and gas phase. The coupling takes place on a micro scale and is difficult to be described due to its dependency on the local geometric structure. However, a smeared continuum model is sufficient for engineering purposes. Those models are formulated based on the principles of continuum mechanics in combination with the mixture theory. In most macroscopic models, it is assumed that all constituents fill the entire control space. Based on homogenization/averaging procedures the microscopic effects are considered. In the book of Coussy [12] the basic equations can be found for saturated and partial saturated media. Further examples for such theories can be found in the review article by Schrefler [39] and, e.g., in [42, 43, 40]. A review of the more simpler case of saturated poroelastic media can be found in [35].

Independently which model with which refinement level is used, analytical solutions are restricted to simple geometries because the governing equations for a three-phase material are a set of three coupled partial differential equations. Hence, numerical methods are the usual way to solve engineering problems. Finite element (FEM) formulations can be found, e.g., in [24] or [16]. However, having wave propagation in mind the boundary element method (BEM) may be considered due to its unique feature to model the radiation condition correctly in infinite or semi-infinite domains. Another advantage to be mentioned is the easier meshing of the surface compared to creating a volume mesh for FEM. Unfortunately, these advantages are accompanied by several drawbacks. First, any non-linear effects should be avoided. Second, fundamental solutions have to be found. Third, fully populated system matrices must be handled effectively. The latter point may be treated with so-called fast methods, however this has not been done until now.

The above listed second point is not really a drawback because literature on fundamental solutions exist. Gatmiri and Jabbari [14, 15] firstly published the closed form two and three dimensional quasi-static Green's functions for an unsaturated deformable porous medium. The two dimensional (2D) and three dimensional (3D) thermo–hydro–mechanical fundamental solutions of a multiphase porous media in frequency and time domain are presented by Gatmiri et al. [17] and Maghoul et al. [29], also for the quasi-static case. The closed form time domain fundamental solutions are derived by an analytical inversion of the Laplace domain solutions. In these publications some assumptions on the compressibility of the constituents have been made, especially for the analytical inverse transformation. An explicit 3D Laplace transform fundamental solution for dynamic partially saturated soils has been published by Ashayeri et al. [6]. In this formulation, the solid grains are assumed to be incompressible. The transient 3D fundamental solution is presented by means of an analytical inverse Laplace transform technique, however, for this inverse transformation the dissipation in the compression and shear wave must

be neglected.

The above overview shows only fundamental solutions but no BE formulation. In principle, there is no BE formulation available in literature up to now. But, it must be mentioned that in [5] and [30] boundary integral equations have been formulated. However, no BE formulation nor a numerical realisation has been made.

In the present paper, a 3D time domain boundary element formulation based on collocation is presented. As well the respective fundamental solutions in 3D in Laplace domain are given. They differ from those of Ashayeri et al. [6] such that the compressibility of the grains is taken into account and a different suction-saturation law has been chosen. The singularities of these fundamental solutions are briefly discussed. A regularization based on partial integration of the strong singular fundamental solution is proposed following the approach presented in [31]. Next, the BE formulation is introduced by deriving the respective boundary integral equation. After the spatial discretisation the time discretisation is done with the Convolution Quadrature Method (CQM), which requires only Laplace domain fundamental solutions. A validation example with a 1D column and two half space computations close the paper.

Throughout this work, the indical notation is used. The summation convention is applied over repeated indices and Latin indices receive the values 1, 2, 3 in 3D. Commas $()_{,i}$ or ∂_i denote spatial derivatives and ∂_t denote the time derivative. The symbol δ_{ij} is the Kronecker-Delta. The Laplace transform of a function $f(t)$ is denoted by $\hat{f}(s)$ with the complex Laplace parameter $s \in \mathbb{C}$ s.t. $\Re s > 0$. It should be remarked that at several places in this paper details are skipped for the sake of readability. These details may be found in the thesis of the first author [25], which is freely available as pdf-file or can be purchased as hard copy.

2 Governing Equations

For dynamic partially saturated poroelasticity the governing equations are stated following the work of Lewis and Schrefler [24]. The essential assumptions are:

- a mixture of the solid phase (solid skeleton), wetting fluid phase (e.g., pore water), and non–wetting phase (e.g., pore air) is considered
- a state transformation of the three phases is not allowed during the fluids infiltration into the solid skeleton
- the evaporation of the wetting fluid and dissolving of non–wetting fluid into wetting fluid is neglected
- all three phases have the same temperature and any temperature change is ignored
- all three phases are compressible.

In the following, only a brief overview with the essential equations is given because further details can be found in [26, 25].

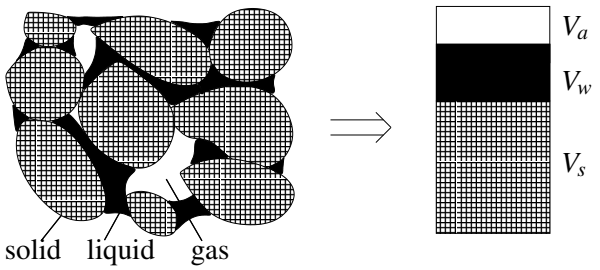

Figure 1: Volume averaging of a partially saturated continuum

2.1 Constitutive assumptions

For a partially saturated porous medium, the porosity n measures the void space, which is the ratio of the volume of voids V_{void} over the total volume V_{total}

$$n = \frac{V_{void}}{V_{total}} \, . \tag{1}$$

The voids are filled with a mixture of fluids, for instance, a mixture of water and air in soil mechanics, or a mixture of oil and water in petroleum engineering (see figure 1) The saturation degrees are defined as the ratios of the volume occupied by the fluid V_w or V_a to the void volume, i.e., it holds

$$S_w = \frac{V_w}{V_{void}} \quad S_a = \frac{V_a}{V_{void}} \qquad S_w + S_a = 1 \, . \tag{2}$$

The capillary pressure p^c in a partially saturated media is given following Brooks and Corey [9]

$$p^c = p^a - p^w = p^d S_e^{-1/\vartheta} \, , \tag{3}$$

where p^d is the non-wetting fluid entry pressure and ϑ is the pore size distribution index. S_e denotes the effective wetting fluid saturation degree

$$S_e = \begin{cases} 0 & S_w \leq S_{rw} \\ \dfrac{S_w - S_{rw}}{S_{ra} - S_{rw}} & S_{rw} < S_w < S_{ra} \\ 1 & S_w \geq S_{ra} \end{cases} \, , \tag{4}$$

where S_{rw} is the residual wetting fluid saturation and S_{ra} is the non-wetting fluid entry saturation.

Following the ideas of Bishop and Blight [8], the total stress σ_{ij} is expressed by [44]

$$\sigma_{ij} = \sigma'_{ij} - \delta_{ij}\alpha(S_w p^w + S_a p^a) \, , \tag{5}$$

where σ'_{ij} denotes the effective stress, $\alpha = 1 - K/K_s$ describes the compressibility of the solid skeleton with the drained bulk modulus of the mixture K and K_s is the bulk modulus of the solid skeleton. The introduction of the factor α is used to describe the compressibility of the solid grains, while $\alpha = 1$ fits to the incompressible case. Assuming an elastic isotropic material for the skeleton, the constitutive model is

$$\sigma'_{ij} = (K - \frac{2}{3}G)\delta_{ij}u_{k,k} + G(u_{i,j} + u_{j,i}) \, , \tag{6}$$

with G denoting the shear modulus. Further, in (6) a linear stress-strain relation is assumed.

2.2 Balance equations

The balances of mass for the solid and both fluids are

$$\partial_t[(1-n)\rho_s] + (1-n)\rho_s \partial_t u_{i,i} = 0 \tag{7a}$$

$$\partial_t(nS_f\rho_f) + nS_f\rho_f\partial_t(u_{i,i} + u^f_{i,i}) = 0 \tag{7b}$$

where ρ_s and $\rho_f (f = w,a)$ denote the density of the solid and the fluids, respectively. Note that in (7b), and also in the following, with the index f the equations of both fluids are summarized. The displacements $u^f (f = w,a)$ are the relative displacement of the fluids according to the solid. In the balances of mass (7) it is assumed that the dissolved non-wetting fluid into the wetting fluid can be neglected. Further, due to the linearization the gradients of the porosity, the densities, and the saturation degrees vanish.

The momentum balance equation for the mixture is the sum of the equations for each individual constituent. Taking into account the constitutive assumption for the total stress (5), the momentum balance equation for the mixture is given by

$$Gu_{i,jj} + (K + \frac{G}{3})u_{j,ij} - \alpha(S_w p^w_{,i} + S_a p^a_{,i}) + F_i = \rho\partial_t^2 u_i + nS_w\rho_w\partial_t^2 u^w_i + nS_a\rho_a\partial_t^2 u^a_i \,, \tag{8}$$

where F_i denotes the bulk body force. The bulk density ρ is the averaged density of the mixture $\rho = (1-n)\rho_s + nS_w\rho_w + nS_a\rho_a$.

The momentum balance equations for each fluid phase yield the generalized form of Darcy's law

$$nS_f\partial_t u^f_i = -\kappa_f \left(p^f_{,i} + \rho_f\partial_t^2 u_i + \rho_f\partial_t^2 u^f_i \right) \quad , \tag{9}$$

where the phase permeability of the wetting fluid ($f = w$) and the non–wetting fluid ($f = a$) is given by $\kappa_f = K_{rf}k/\eta_f \quad (f = w,a)$. K_{rf} denotes the relative fluid phase permeability, k denotes the intrinsic fluid permeability of a porous continuum, and η_f is the viscosity of the fluid.

The relative phase permeability K_{rf} is a dimensionless measure of the effective permeability of the f-phase. It is the ratio of the effective permeability of the f-phase to the absolute permeability. Based on experiments, the relative permeability can be constructed as a function of the saturation degree. According to the literature, the relative permeability K_{rf} can be evaluated either following the method of Brooks and Corey [9] or van Genuchten [41]. In the following, the equations of the relative permeability by Brooks and Corey are used and are given by

$$K_{rw} = S_e^{(2+3\vartheta)/\vartheta} \qquad K_{ra} = (1-S_e)^2 \left[1 - S_e^{(2+\vartheta)/\vartheta}\right] \,. \tag{10}$$

These empirical equations are based on the experiment of a water–gas mixture. For other mixtures, e.g., a mixture of water–oil or oil–gas, the corresponding empirical equations are needed.

2.3 Governing equations in the Laplace domain

Equations (7), (8), and (9) are sufficient to solve the problem of partially saturated poroelasticity. From a physical point of view, the solid displacement and both pore pressures are a useful set of unknowns. This requires an elimination of the relative displacements. In time domain, however,

this is not possible, because they appear in (7), (8), and (9) in different orders of time derivatives. Hence, the Laplace transformation is introduced to eliminate the time derivatives.

Applying the Laplace transformation to (9) and rearranging it with respect to the relative displacement $\hat{u}_i^f$ gives

$$\hat{q}_i^w = s\hat{u}_i^w = -\frac{\beta}{n\rho_w s}\left(\hat{p}_{,i}^w + \rho_w s^2 \hat{u}_i\right) \qquad \hat{q}_i^a = s\hat{u}_i^a = -\frac{\gamma}{n\rho_a s}\left(\hat{p}_{,i}^a + \rho_a s^2 \hat{u}_i\right) , \tag{11}$$

where $\hat{q}_i^f\,(f = w,a)$ denotes the wetting fluid / non–wetting fluid flux, respectively. Further, the Laplace parameter dependent abbreviations

$$\beta = \frac{\kappa_w n \rho_w s}{nS_w + \kappa_w \rho_w s} \qquad \gamma = \frac{\kappa_a n \rho_a s}{nS_a + \kappa_a \rho_a s} \tag{12}$$

are introduced.

Substituting the relative displacements (11) in (7) and (8), the governing equations of partially saturated poroelasticity in the Laplace domain are obtained

$$G\hat{u}_{i,jj} + (K + \frac{G}{3})\hat{u}_{j,ij} - (\rho - \beta S_w \rho_w - \gamma S_a \rho_a)s^2 \hat{u}_i - (\alpha - \beta)S_w \hat{p}_{,i}^w - (\alpha - \gamma)S_a \hat{p}_{,i}^a = -\hat{F}_i \tag{13a}$$

$$-(\alpha - \beta)S_w s\hat{u}_{i,i} - (\zeta S_{ww} S_w + \frac{n}{K_w}S_w - S_u)s\hat{p}^w + \frac{\beta S_w}{\rho_w s}\hat{p}_{,ii}^w - (\zeta S_{aa} S_w + S_u)s\hat{p}^a = -\hat{I}^w \tag{13b}$$

$$-(\alpha - \gamma)S_a s\hat{u}_{i,i} - (\zeta S_{ww} S_a + S_u)s\hat{p}^w - (\zeta S_{aa} S_a + \frac{n}{K_a}S_a - S_u)s\hat{p}^a + \frac{\gamma S_a}{\rho_a s}\hat{p}_{,ii}^a = -\hat{I}^a , \tag{13c}$$

with the abbreviations

$$\zeta = \frac{\alpha - n}{K_s} \quad S_{ww} = S_w - \vartheta(S_w - S_{rw}) \quad S_{aa} = S_a + \vartheta(S_w - S_{rw})$$

$$S_u = -\frac{\vartheta(S_{ra} - S_{rw})}{p^d}\left(\frac{S_w - S_{rw}}{S_{ra} - S_{rw}}\right)^{\frac{\vartheta+1}{\vartheta}} .$$

As already mentioned, a more detailed derivation of the governing equations can be found in [26, 25].

A more compact notation of the coupled differential equations (13) is

$$\underbrace{\begin{bmatrix} A_1\delta_{ij} + A_2\partial_i\partial_j & A_3\partial_i & A_4\partial_i \\ A_5\partial_j & A_6 & A_7 \\ A_8\partial j & A_9 & A_{10} \end{bmatrix}}_{\mathcal{B}} \begin{bmatrix} \hat{u}_i \\ \hat{p}^w \\ \hat{p}^a \end{bmatrix} = \begin{bmatrix} -\hat{F}_i \\ -\hat{I}^w \\ -\hat{I}^a \end{bmatrix} \tag{14}$$

with the not self-adjoint operator $\mathcal{B}$. The explicite forms of A_1–A_{10} can be found in A.1.

Remark 1: In the above derived governing equations, a constant spatial distribution of the saturation degree is explicitly assumed. However, it should be remarked that this holds only for the initial saturation degree. This initial saturation degree could be equal to or within the range

of the irreducible saturation degree, which is a minimum saturation degree in a porous medium. Therefore, the application of the proposed model is constrained.

Remark 2: The presented governing equations can only describe the properties of partially saturated poroelasticity when $0 < S_w < 1$. For the extreme cases, $S_w = 0$ or $S_w = 1$, the equations turn out to be the governing equations of saturated poroelasticity either with air or water in the pores.

3 Fundamental Solutions

In order to establish the boundary integral equation related to the set of coupled differential equations (13), one crucial condition is the knowledge of corresponding fundamental solutions.

3.1 Derivation with Hörmander's method

For usage of fundamental solutions in a boundary integral equation, the adjoint problem to the coupled set of differential equations (13) have to be solved with a Dirac distribution as inhomogeneity for every degree of freedom. Hence, the fundamental solution $\hat{\mathbf{U}} = \hat{\mathbf{U}}(\mathbf{x},\mathbf{y})$ of the differential operator $\mathcal{B}$ is

$$\mathcal{B}^* \, \hat{\mathbf{U}} + \mathbf{I}\delta(\mathbf{x},\mathbf{y}) = \mathbf{0} \quad , \tag{15}$$

where $\mathcal{B}^*$ is the adjoint operator of $\mathcal{B}$ in (14). Its explicit expression can easily be obtained by building the transpose of the operator and adding at the off-diagonal terms negative signs. These negative signs come from the first order partial derivative. $\mathbf{I}$ denotes the identity matrix and $\delta(\mathbf{x},\mathbf{y})$ the Dirac distribution.

Following Hörmander's method [20], the ansatz

$$\hat{\mathbf{U}} = \mathcal{B}^{*co}\varphi \tag{16}$$

is made, where $\mathcal{B}^{*co}$ denotes the co–factors of $\mathcal{B}^*$ defined via $\mathcal{B}^{*co} = \det(\mathcal{B}^*)\mathcal{B}^{*-1}$ and φ is a yet unknown scalar function. Inserting the ansatz in (15) requires to find the solution φ of the scalar equation

$$\det(\mathcal{B}^*)\varphi + \delta(\mathbf{x},\mathbf{y}) = 0 \, . \tag{17}$$

The determinant of the adjoint operator is

$$\det(\mathcal{B}^*) = (K + \frac{4}{3}G)\frac{G^2\beta\gamma S_w S_a}{\rho_w \rho_a s^2}(\nabla^2 - \lambda_1^2)(\nabla^2 - \lambda_2^2)(\nabla^2 - \lambda_3^2)(\nabla^2 - \lambda_4^2)^2 \, , \tag{18}$$

with ∇ denoting the Nabla-operator. The roots λ_i of the characteristic equation can be deter-

mined to

$$\lambda_1^2 = -\frac{1}{3}\left(D_1 + \sqrt[3]{\frac{m+\sqrt{n}}{2}} + \sqrt[3]{\frac{m-\sqrt{n}}{2}}\right) \tag{19a}$$

$$\lambda_2^2 = -\frac{1}{3}\left(D_1 + k_2\sqrt[3]{\frac{m+\sqrt{n}}{2}} + k_1\sqrt[3]{\frac{m-\sqrt{n}}{2}}\right) \tag{19b}$$

$$\lambda_3^2 = -\frac{1}{3}\left(D_1 + k_1\sqrt[3]{\frac{m+\sqrt{n}}{2}} + k_2\sqrt[3]{\frac{m-\sqrt{n}}{2}}\right) \tag{19c}$$

$$\lambda_4^2 = \frac{\rho - \beta S_w \rho_w - \gamma S_a \rho_a}{G} s^2 \quad , \tag{19d}$$

with $m = 2D_1^3 - 9D_1D_2 + 27D_3$, $n = m^2 - 4(D_1^2 - 3D_2)^3$, $k_1 = \dfrac{-1+i\sqrt{3}}{2}$, $k_2 = \dfrac{-1-i\sqrt{3}}{2}$ and the D_i given in A.1. The four roots correspond to the three compressional waves and the shear wave, which exist in a partially saturated porous media. Obviously, the last (19d) correspond to the shear wave. All roots are frequency, respectively time dependent. The scalar function φ is essentially the solution of a higher order Helmholtz equation given by [11]

$$\begin{aligned}\Psi = -\frac{1}{4\pi r}\Bigg[&\frac{e^{i\lambda_1 r}}{(\lambda_2^2-\lambda_1^2)(\lambda_3^2-\lambda_1^2)(\lambda_4^2-\lambda_1^2)} + \frac{e^{i\lambda_2 r}}{(\lambda_1^2-\lambda_2^2)(\lambda_3^2-\lambda_2^2)(\lambda_4^2-\lambda_2^2)} \\ &+ \frac{e^{i\lambda_3 r}}{(\lambda_1^2-\lambda_3^2)(\lambda_2^2-\lambda_3^2)(\lambda_4^2-\lambda_3^2)} + \frac{e^{i\lambda_4 r}}{(\lambda_1^2-\lambda_4^2)(\lambda_2^2-\lambda_4^2)(\lambda_3^2-\lambda_4^2)}\Bigg]\end{aligned} \tag{20}$$

in combination with

$$\Psi = (K + \frac{4}{3}G)\frac{G^2\beta\gamma S_w S_a}{\rho_w \rho_a s^2}(\nabla^2 - \lambda_4^2)\varphi \, . \tag{21}$$

The last step is to apply the operator

$$\mathcal{B}^{*co} = A_1 \begin{bmatrix} (X_1 - X_2\nabla^2)\delta_{ij} + X_2\partial_{ij} & X_3\partial_i & X_4\partial_i \\ X_5\partial_j & X_7 & X_8 \\ X_6\partial_j & X_9 & X_{10} \end{bmatrix} \tag{22}$$

on the function φ following the ansatz (16). The explicit forms of the symbols X_i in (22) can be found in A.1. This results in the fundamental solutions for partially saturated poroelasticity

$$\begin{aligned}\hat{\mathbf{U}} &= \begin{bmatrix} \hat{U}_{ij}^{ss} & \hat{U}_i^{ws} & \hat{U}_i^{as} \\ \hat{P}_j^{sw} & \hat{P}^{ww} & \hat{P}^{aw} \\ \hat{P}_j^{sa} & \hat{P}^{wa} & \hat{P}^{aa} \end{bmatrix} \\ &= \frac{\rho_w \rho_a s^2}{G\beta\gamma S_w S_a (K + 4G/3)} \begin{bmatrix} (X_1 - X_2\nabla^2)\delta_{ij} + X_2\partial_{ij} & X_3\partial_i & X_4\partial_i \\ X_5\partial_j & X_7 & X_8 \\ X_6\partial_j & X_9 & X_{10} \end{bmatrix} \Psi \, .\end{aligned} \tag{23}$$

The matrix of fundamental solutions (23) consist of nine parts, the displacement and the pore pressure fundamental solutions $\hat{U}_{ij}^{ss}$, $\hat{P}^{ww}$, $\hat{P}^{aa}$, and the six coupling entries. To compute all

entries the operator have to be applied on Ψ, which is preferably done with some symbolic mathematical program. The final results for (23) and the traction and flux fundamental solutions are presented in A.2. Exemplarily, the displacement fundamental solution is

$$\hat{U}_{ij}^{ss} = \frac{w_0}{4\pi r^3} \sum_{m=1}^{4} w_m \left[r_{,i} r_{,j} R_m (\lambda_m^2 r^2 + 3\lambda_m r + 3) + \delta_{ij} (S_m r^2 - R_m \lambda_m r - R_m) \right] \quad , \tag{24}$$

where the abbreviations can be found also in A.2. For the interpretation of the sum the abbreviation

$$w_m = \frac{e^{-\lambda_m r}}{\prod_{j=1, j\neq m}^{4} (\lambda_m^2 - \lambda_j^2)}$$

has to be considered. It shows that the summation relates the four entries to the four waves.

Remark 3: The derived fundamental solutions for partially saturated poroelasticity are comparable with the solutions by Ashayeri et al. [6]. The most obvious difference in the material model is the incompressibility assumption for the solid grains in [6], which is not made in the formulation presented here.

3.2 Singular behavior

The fundamental solutions are by definition singular functions for $r = |\mathbf{x} - \mathbf{y}| \to 0$. The order of the singularity must be known for using those solutions in boundary integral equations. The determination of the singularity can mostly be done by a series expansion with respect to r. In the above given solution the power series representation of the exponential function in Ψ can be used. Finally, it is found that $\hat{U}_{ij}^{ss}, \hat{P}^{ww}$, and $\hat{P}^{aa}$ behave like $O\left(r^{-1}\right)$ and the coupling terms are regular.

For later use it makes sense to look closer on the expression for $\hat{\mathbf{U}}^{ss}$. It can be decomposed into a singular part $\hat{\mathbf{U}}_{sing}$ and a regular part $\hat{\mathbf{U}}_{reg}$

$$\hat{\mathbf{U}}^{ss} = \hat{\mathbf{U}}_{sin} + \hat{\mathbf{U}}_{reg} \ , \tag{25}$$

where both terms are

$$\hat{\mathbf{U}}_{sin} = \frac{1}{G} \left(\nabla^2 \mathbf{I} - \frac{3K+G}{3K+4G} \nabla \nabla^\top \right) \nabla^4 \Psi \tag{26a}$$

$$\begin{aligned} \hat{\mathbf{U}}_{reg} = &- \frac{1}{G} \left[(\lambda_1^2 + \lambda_2^2 + \lambda_3^2) \nabla^4 - (\lambda_1^2 \lambda_2^2 + \lambda_1^2 \lambda_3^2 + \lambda_2^2 \lambda_3^2) \nabla^2 + \lambda_1^2 \lambda_2^2 \lambda_3^2 \right] \mathbf{I} \Psi \\ &+ w_0 (r_6 \nabla^2 + r_7) \nabla \nabla^\top \Psi \ . \end{aligned} \tag{26b}$$

The singular behavior becomes obvious if the structure of Ψ in (20) is considered. Only the application of ∇^4 on Ψ in combination with ∇^2 or $\nabla \nabla^\top$ gives a singular solution. The term $\hat{\mathbf{U}}_{sing}$ has exactly the same structure as the elastostatic kernel where Ψ is the only difference. Further, for saturated poroelasticity the same form also only differing in Ψ can be observed. This can be used to regularize the traction kernel following the lines given in [31]. Based on the constitutive equation (5) the traction fundamental solution can be written as

$$\hat{\mathbf{T}}^{ss} = \hat{\mathcal{T}}^e \hat{\mathbf{U}}^{ss} + s\alpha (S_w \hat{\mathbf{P}}^{sw} \mathbf{n}^\top + S_a \hat{\mathbf{P}}^{sa} \mathbf{n}^\top) \ . \tag{27}$$

Inserting the splitting of the displacement fundamental solution (26) allows to split the traction as well in a singular and a regular part

$$\begin{aligned}\hat{\mathbf{T}}^{ss} &= \hat{T}^e(\hat{\mathbf{U}}_{sin} + \hat{\mathbf{U}}_{reg}) + \alpha s(S_w\hat{\mathbf{P}}^{sw} + S_a\hat{\mathbf{P}}^{sa})\mathbf{n}^\top \\ &= \hat{T}^e\hat{\mathbf{U}}_{sin} + O(r^0)\ .\end{aligned} \tag{28}$$

Above the operator $\hat{T}^e$ is the elastic traction operator or in other words Hooke's law of elasticity (see (6)). Equation (28) shows that the singularity of the traction fundamental solution is the same as in saturated poroelasticity and, hence, the regularization proposed in [31] can be used in the boundary integral equation.

As mentioned above the pressure fundamental solutions $\hat{P}^{ww}$ and $\hat{P}^{aa}$ behave like $O\left(r^{-1}\right)$ and have the same form in the limit $r \to 0$ as in acoustics. Hence, also the flux fundamental solutions behave like the flux in acoustics and must not be treated separately.

3.3 Visualization in time domain

The displacement $\hat{U}_{ij}^{ss}$ and pore pressure fundamental solutions $\hat{P}^{ww}$, $\hat{P}^{aa}$ are calculated to visualize the principle behavior of the partially saturated poroelastic model. Not the solutions in Laplace domain are presented but the time domain results. These are calculated using the convolution quadrature method [27, 28]. Further, not the impulse response functions are presented but the response due to a Heaviside time history for the load. This is realized by the convolution between the fundamental solution and the Heaviside function. Massilon Sandstone (see [33]) is chosen as material for the calculation. The used material parameters are listed in table 1. Beside,

Table 1: Parameters of Massilon sandstone (from [33])

Parameter type	Symbol	Value	Unit
Porosity	n	0.23	-
Density of the solid skeleton	ρ_s	2650	$\mathrm{kg/m^3}$
Density of the water	ρ_w	997	$\mathrm{kg/m^3}$
Density of the air	ρ_a	1.10	$\mathrm{kg/m^3}$
Drained bulk modulus of the mixture	K	1.02×10^9	$\mathrm{N/m^2}$
Shear modulus of the mixture	G	1.44×10^9	$\mathrm{N/m^2}$
Bulk modulus of the solid grains	K_s	3.5×10^{10}	$\mathrm{N/m^2}$
Bulk modulus of the water	K_w	2.25×10^9	$\mathrm{N/m^2}$
Bulk modulus of the air	K_a	1.10×10^5	$\mathrm{N/m^2}$
Intrinsic permeability	k	2.5×10^{-12}	$\mathrm{m^2}$
Viscosity of the water	η_w	1.0×10^{-3}	$\mathrm{Ns/m^2}$
Viscosity of the air	η_a	1.8×10^{-5}	$\mathrm{Ns/m^2}$
Gas entry pressure	p^d	5×10^4	$\mathrm{N/m^2}$

the pore size distribution index ϑ is set to 1.5, the residual water saturation S_{rw} is set to 0, and the air entry saturation S_{ra} is set to 1.

In figure 2 and 3, the time dependent displacement and pore pressure responses are depicted versus time for different water saturations S_w at the distance $r = 0.5\,\mathrm{m}$, i.e., $\mathbf{x} = [0.5, 0, 0]$ and $\mathbf{y} = [0, 0, 0]$. The chosen water saturations are $S_w = 0.60$, $S_w = 0.80$ and $S_w = 0.95$. The

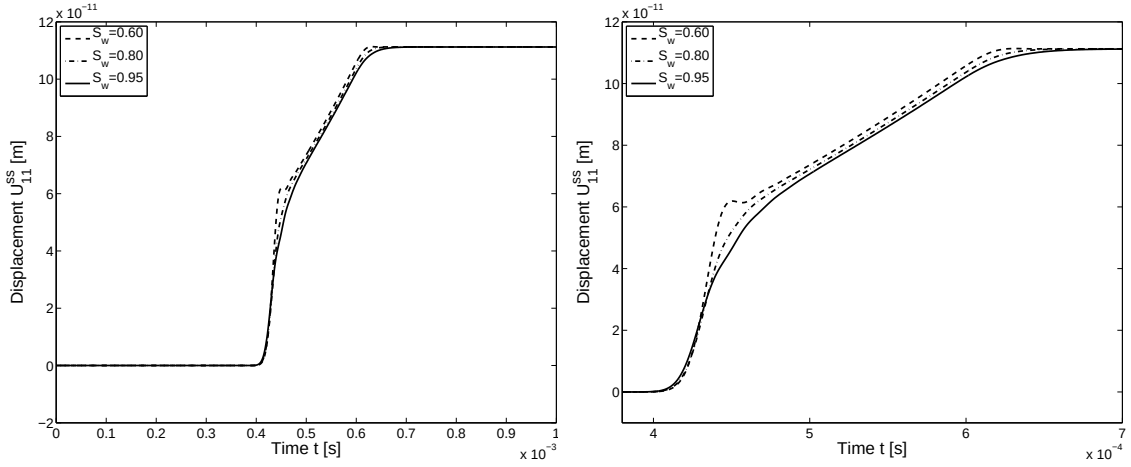

(a) Full scale (b) Zoom

Figure 2: Displacement U_{11}^{ss} versus time with varying saturation degree at $r = 0.5\,\mathrm{m}$

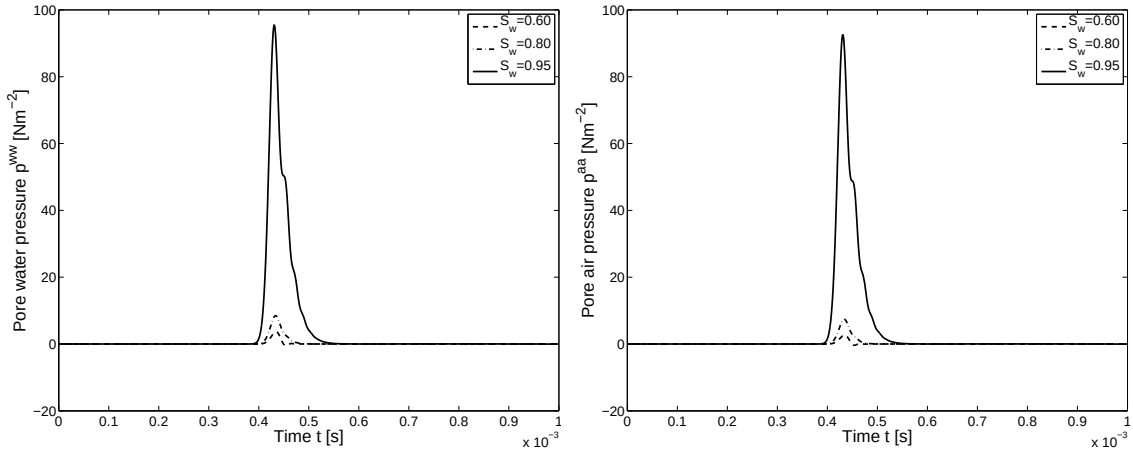

(a) Pore water pressure (b) Pore air pressure

Figure 3: Pore pressure versus time with varying saturation degree at $r = 0.5\,\mathrm{m}$

jump around $t = 0.00043\,\mathrm{s}$ in figure 2b corresponds to the fast compressional wave, however, the expected jump due to the arrival of the shear wave is not very obvious. This might be caused by the chosen values for r and $r_{,i}$. The value of the displacement decreases with increasing the water saturation S_w, however, the differences of the three unsaturated cases are quite small.

Both, the pore water and pore air pressure are shown in figure 3. The pore pressures are

mostly zero in the given time period except for the arrival of the fast compressional wave. The values of the pore water and pore air pressure increase with increasing the water saturation S_w.

Overall, in both figures the slow compressional waves are not visible due to the strong damping of these waves.

4 Boundary Element Formulation

4.1 Boundary integral equation

To derive an integral equation corresponding to (13) the method of weighted residuals can be used. As usual, the fundamental solutions $\hat{\mathbf{U}}$ are used as weighting functions. Hence, in a domain Ω with boundary Γ it holds

$$\int_\Omega \hat{\mathbf{U}}^\top \mathcal{B}\, \hat{\mathbf{u}}\, d\Omega = \mathbf{0}\,. \tag{29}$$

Introducing the explicit expressions of the fundamental solutions $\hat{\mathbf{U}}$ from (23) and applying the partial differential operator $\mathcal{B}$, the integral equation (29) is expanded into

$$\int_\Omega (\hat{U}^{ss}_{ij} I_1 + \hat{P}^{sw}_j I_2 + \hat{P}^{sa}_j I_3)\, d\Omega = 0 \tag{30a}$$

$$\int_\Omega (\hat{U}^{ws}_{i} I_1 + \hat{P}^{ww} I_2 + \hat{P}^{wa} I_3)\, d\Omega = 0 \tag{30b}$$

$$\int_\Omega (\hat{U}^{as}_{i} I_1 + \hat{P}^{aw} I_2 + \hat{P}^{aa} I_3)\, d\Omega = 0 \quad , \tag{30c}$$

with the explicit expressions

$$\begin{aligned}
I_1 =& G\hat{u}_{i,kk} - (\rho - \beta S_w \rho_w - \gamma S_a \rho_a) s^2 \hat{u}_i + (K + \frac{G}{3})\hat{u}_{k,ik} - (\alpha - \beta) S_w \hat{P}^w_{,i} - (\alpha - \gamma) S_a \hat{P}^a_{,i} \\
I_2 =& -(\alpha - \beta) S_w s \hat{u}_{k,k} - (\zeta S_{ww} S_w + \frac{n}{K_w} S_w - S_u) s \hat{P}^w + \frac{\beta S_w}{\rho_w s} \hat{P}^w_{,kk} - (\zeta S_{aa} S_w + S_u) s \hat{P}^a \\
I_3 =& -(\alpha - \gamma) S_a s \hat{u}_{k,k} - (\zeta S_{ww} S_a + S_u) s \hat{P}^w - (\zeta S_{aa} S_a + \frac{n}{K_a} S_a - S_u) s \hat{P}^a + \frac{\gamma S_a}{\rho_a s} \hat{P}^a_{,kk}\,.
\end{aligned}$$

In the integral equations (30) either one or two differentiations have to be transformed from $\hat{\mathbf{u}}$ to the fundamental solutions by either one or two partial integrations. Exemplarily, two parts of the proposed integral equations (30) are presented in detail to show the principal procedure. All other partial integrations for the other parts in the integral equations can be performed analogously.

First, an integral with one differentiation in the integral equation (30b) is transformed by one partial integration

$$\begin{aligned}
\int_\Omega (\alpha - \beta) S_w s \hat{u}_{k,k} \hat{P}^{ww} d\Omega &= \int_\Omega (\alpha - \beta) S_w s (\hat{u}_k \hat{P}^{ww})_{,k} d\Omega - \int_\Omega (\alpha - \beta) S_w s \hat{u}_k \hat{P}^{ww}_{,k} d\Omega \\
&= \int_\Gamma (\alpha - \beta) S_w s \hat{u}_k n_k \hat{P}^{ww} d\Gamma - \int_\Omega (\alpha - \beta) S_w s \hat{u}_k \hat{P}^{ww}_{,k} d\Omega
\end{aligned}$$

where n_k is the outward normal vector on the boundary Γ. Second, an integral with two differentiation in the integral equation (30a) is transformed by two partial integrations

$$\begin{aligned}\int_\Omega G\hat{u}_{i,kk}\hat{U}^{ss}_{ij} &= \int_\Omega G(\hat{u}_{i,k}\hat{U}^{ss}_{ij})_{,k}d\Omega - \int_\Omega G\hat{u}_{i,k}\hat{U}^{ss}_{ij,k}d\Omega = \int_\Gamma G\hat{u}_{i,k}n_k\hat{U}^{ss}_{ij}d\Gamma - \int_\Omega G\hat{u}_{i,k}\hat{U}^{ss}_{ij,k}d\Omega \\ &= \int_\Gamma G\hat{u}_{i,k}n_k\hat{U}^{ss}_{ij}d\Gamma - \int_\Omega G(\hat{u}_i\hat{U}^{ss}_{ij,k})_{,k}d\Omega + \int_\Omega G\hat{u}_i\hat{U}^{ss}_{ij,kk}d\Omega \\ &= \int_\Gamma G\hat{u}_{i,k}n_k\hat{U}^{ss}_{ij}d\Gamma - \int_\Gamma G\hat{u}_i\hat{U}^{ss}_{ij,k}n_k d\Gamma + \int_\Omega G\hat{u}_i\hat{U}^{ss}_{ij,kk}d\Omega\,.\end{aligned}$$

The transformation from the domain to the boundary integral is performed with the divergence theorem. Obviously, one integration by parts changes the sign of the resulting domain integral, while it remains unchanged in the case of two integration by parts, i.e., the differential operator $\mathcal{B}$ is transformed into its adjoint operator $\mathcal{B}^*$.

This yields the following integral equation given in matrix notation

$$\int_\Gamma \begin{bmatrix} \hat{U}^{ss}_{ij} & -\hat{P}^{sw}_j & -\hat{P}^{sa}_j \\ \hat{U}^{ws}_i & -\hat{P}^{ww} & -\hat{P}^{wa} \\ \hat{U}^{as}_i & -\hat{P}^{aw} & -\hat{P}^{aa} \end{bmatrix} \begin{bmatrix} \hat{t}_i \\ \hat{q}^w \\ \hat{q}^a \end{bmatrix} d\Gamma - \int_\Gamma \begin{bmatrix} \hat{T}^{ss}_{ij} & \hat{Q}^{sw}_j & \hat{Q}^{sa}_j \\ \hat{T}^{ws}_i & \hat{Q}^{ww} & \hat{Q}^{wa} \\ \hat{T}^{as}_i & \hat{Q}^{aw} & \hat{Q}^{aa} \end{bmatrix} \begin{bmatrix} \hat{u}_i \\ \hat{p}^w \\ \hat{p}^a \end{bmatrix} d\Gamma = \begin{bmatrix} \hat{u}_j \\ \hat{p}^w \\ \hat{p}^a \end{bmatrix}, \tag{31}$$

where the property $\mathcal{B}^*\hat{U}_{ij} = -\delta(\mathbf{x},\mathbf{y})\delta_{ij}$ has been used. The abbreviations of the traction and flux fundamental solutions can be found in A.2. Additional to the definition of the flux from (11), the total traction vector $\hat{t}_i = \hat{\sigma}_{ij}n_j$ has been used.

The last step in the derivation of a boundary integral equation is to move the load point $\mathbf{y}$ to the boundary. This follows the usual steps, which can be found in any text book on BEM. The procedure is exactly the same as in elastostatics because the strong singularity is the same. The flux kernel needs no special treatment. Finally, the explicit expressions of the boundary integral equations are given by

$$\begin{aligned}\int_\Gamma \begin{bmatrix} \hat{U}^{ss}_{ij} & \hat{P}^{sw}_j & \hat{P}^{sa}_j \\ \hat{U}^{ws}_i & \hat{P}^{ww} & \hat{P}^{wa} \\ \hat{U}^{as}_i & \hat{P}^{aw} & \hat{P}^{aa} \end{bmatrix} \begin{bmatrix} \hat{t}_i \\ -\hat{q}^w \\ -\hat{q}^a \end{bmatrix} d\Gamma - \oint_\Gamma \begin{bmatrix} \hat{T}^{ss}_{ij} & \hat{Q}^{sw}_j & \hat{Q}^{sa}_j \\ \hat{T}^{ws}_i & \hat{Q}^{ww} & \hat{Q}^{wa} \\ \hat{T}^{as}_i & \hat{Q}^{aw} & \hat{Q}^{aa} \end{bmatrix} \begin{bmatrix} \hat{u}_i \\ \hat{p}^w \\ \hat{p}^a \end{bmatrix} d\Gamma \\ = \begin{bmatrix} c_{ij} & 0 & 0 \\ 0 & c & 0 \\ 0 & 0 & c \end{bmatrix} \begin{bmatrix} \hat{u}_i \\ \hat{p}^w \\ \hat{p}^a \end{bmatrix},\end{aligned} \tag{32}$$

where the integral in the sense of a Cauchy Principal Value is marked with the symbol $\oint$. This is only necessary for the entry $\hat{T}^{ss}_{ij}$. The integral free terms c_{ij} and c are defined as in elastostatics or acoustics, respectively.

Next, the time dependent boundary integral equations are obtained by a formal inverse Laplace

transformation

$$\begin{aligned}
&\int_0^t \int_\Gamma \begin{bmatrix} U_{ij}^{ss}(t-\tau,\mathbf{y},\mathbf{x}) & P_j^{sw}(t-\tau,\mathbf{y},\mathbf{x}) & P_j^{sa}(t-\tau,\mathbf{y},\mathbf{x}) \\ U_i^{ws}(t-\tau,\mathbf{y},\mathbf{x}) & P^{ww}(t-\tau,\mathbf{y},\mathbf{x}) & P^{wa}(t-\tau,\mathbf{y},\mathbf{x}) \\ U_i^{as}(t-\tau,\mathbf{y},\mathbf{x}) & P^{aw}(t-\tau,\mathbf{y},\mathbf{x}) & P^{aa}(t-\tau,\mathbf{y},\mathbf{x}) \end{bmatrix} \begin{bmatrix} t_i(\tau,\mathbf{x}) \\ -q^w(\tau,\mathbf{x}) \\ -q^a(\tau,\mathbf{x}) \end{bmatrix} d\Gamma d\tau \\
&- \int_0^t \oint_\Gamma \begin{bmatrix} T_{ij}^{ss}(t-\tau,\mathbf{y},\mathbf{x}) & Q_j^{sw}(t-\tau,\mathbf{y},\mathbf{x}) & Q_j^{sa}(t-\tau,\mathbf{y},\mathbf{x}) \\ T_i^{ws}(t-\tau,\mathbf{y},\mathbf{x}) & Q^{ww}(t-\tau,\mathbf{y},\mathbf{x}) & Q^{wa}(t-\tau,\mathbf{y},\mathbf{x}) \\ T_i^{as}(t-\tau,\mathbf{y},\mathbf{x}) & Q^{aw}(t-\tau,\mathbf{y},\mathbf{x}) & Q^{aa}(t-\tau,\mathbf{y},\mathbf{x}) \end{bmatrix} \begin{bmatrix} u_i(\tau,\mathbf{x}) \\ p^w(\tau,\mathbf{x}) \\ p^a(\tau,\mathbf{x}) \end{bmatrix} d\Gamma d\tau \\
&= \begin{bmatrix} c_{ij}(\mathbf{y}) & 0 & 0 \\ 0 & c(\mathbf{y}) & 0 \\ 0 & 0 & c(\mathbf{y}) \end{bmatrix} \begin{bmatrix} u_i(t,\mathbf{y}) \\ p^w(t,\mathbf{y}) \\ p^a(t,\mathbf{y}) \end{bmatrix} \quad .
\end{aligned} \tag{33}$$

Treatment of singular integrals In the boundary integral equations weak and strong singular exist. As discussed in section 3, terms on the main diagonal of the first integral in (33) are weak singular. The off-diagonal entries in the second integral are as well weak singular, whereas the flux terms does not lead to a strong singularity for smooth enough surfaces [19]. The entry T_{ij}^{ss} is handled by partial integration. This procedure follows the steps from the regularization of saturated poroelasticity as published in [31]. The necessary decomposition is shown in (28). This results in a weak singular integral equation.

4.2 Discretisation

To approximate the geometry, the boundary $\Gamma = \partial\Omega$ is divided into E triangular boundary elements Γ_e via a standard triangulation

$$\Gamma \approx \sum_{e=1}^{E} \Gamma_e \quad . \tag{34}$$

A combination of F continuous or piecewise discontinuous polynomial shape functions $N_e^f(\mathbf{x})$ is defined for the unknown Dirichlet and Neumann datum, respectively. Hence, the following shape functions are used with the time–dependent nodal values $u_i^{ef}(t)$, $t_i^{ef}(t)$, $p^{w^{ef}}(t)$, $q^{w^{ef}}(t)$, $p^{a^{ef}}(t)$, and $q^{a^{ef}}(t)$

$$\begin{aligned}
u_i(\mathbf{x},t) &= \sum_{e=1}^{E}\sum_{f=1}^{F} N_e^f(\mathbf{x}) u_i^{ef}(t) & t_i(\mathbf{x},t) &= \sum_{e=1}^{E}\sum_{f=1}^{F} N_e^f(\mathbf{x}) t_i^{ef}(t) \\
p^w(\mathbf{x},t) &= \sum_{e=1}^{E}\sum_{f=1}^{F} N_e^f(\mathbf{x}) p^{w^{ef}}(t) & q^w(\mathbf{x},t) &= \sum_{e=1}^{E}\sum_{f=1}^{F} N_e^f(\mathbf{x}) q^{w^{ef}}(t) \\
p^a(\mathbf{x},t) &= \sum_{e=1}^{E}\sum_{f=1}^{F} N_e^f(\mathbf{x}) p^{a^{ef}}(t) & q^a(\mathbf{x},t) &= \sum_{e=1}^{E}\sum_{f=1}^{F} N_e^f(\mathbf{x}) q^{a^{ef}}(t) \quad .
\end{aligned} \tag{35}$$

For calculations in the next section, the shape functions of the unknown Dirichlet datum are linear while those of the unknown Neumann datum are constant.

Next, a time discretization has to be introduced. By dividing the time period t in N intervals of equal duration Δt, i.e., $t = N\Delta t$, the convolution integrals between the fundamental solutions and the nodal values are approximated by the CQM. For details about the CQM see either the original work by Lubich [27, 28] or a more applied representation in [37, 36].

Inserting the shape functions (35) and the CQM into the time dependent integral equation (33) yields the following boundary element time stepping formulation for $n = 0, 1, 2, ..., N$

$$\begin{aligned}
&\sum_{e=1}^{E}\sum_{f=1}^{F}\sum_{k=0}^{n}\begin{bmatrix} \omega^{ef}_{n-k}(\hat{U}^{ss}_{ij},\mathbf{y},\Delta t) & \omega^{ef}_{n-k}(\hat{P}^{sw}_{j},\mathbf{y},\Delta t) & \omega^{ef}_{n-k}(\hat{P}^{sa}_{j},\mathbf{y},\Delta t) \\ \omega^{ef}_{n-k}(\hat{U}^{ws}_{i},\mathbf{y},\Delta t) & \omega^{ef}_{n-k}(\hat{P}^{ww},\mathbf{y},\Delta t) & \omega^{ef}_{n-k}(\hat{P}^{wa},\mathbf{y},\Delta t) \\ \omega^{ef}_{n-k}(\hat{U}^{as}_{i},\mathbf{y},\Delta t) & \omega^{ef}_{n-k}(\hat{P}^{aw},\mathbf{y},\Delta t) & \omega^{ef}_{n-k}(\hat{P}^{aa},\mathbf{y},\Delta t) \end{bmatrix}\begin{bmatrix} t^{ef}_{i}(k\Delta t) \\ -q^{w^{ef}}(k\Delta t) \\ -q^{a^{ef}}(k\Delta t) \end{bmatrix} \\
-&\sum_{e=1}^{E}\sum_{f=1}^{F}\sum_{k=0}^{n}\begin{bmatrix} \omega^{ef}_{n-k}(\hat{T}^{ss}_{ij},\mathbf{y},\Delta t) & \omega^{ef}_{n-k}(\hat{Q}^{sw}_{j},\mathbf{y},\Delta t) & \omega^{ef}_{n-k}(\hat{Q}^{sa}_{j},\mathbf{y},\Delta t) \\ \omega^{ef}_{n-k}(\hat{T}^{ws}_{i},\mathbf{y},\Delta t) & \omega^{ef}_{n-k}(\hat{Q}^{ww},\mathbf{y},\Delta t) & \omega^{ef}_{n-k}(\hat{Q}^{wa},\mathbf{y},\Delta t) \\ \omega^{ef}_{n-k}(\hat{T}^{as}_{i},\mathbf{y},\Delta t) & \omega^{ef}_{n-k}(\hat{Q}^{aw},\mathbf{y},\Delta t) & \omega^{ef}_{n-k}(\hat{Q}^{aa},\mathbf{y},\Delta t) \end{bmatrix}\begin{bmatrix} u^{ef}_{i}(k\Delta t) \\ p^{w^{ef}}(k\Delta t) \\ p^{a^{ef}}(k\Delta t) \end{bmatrix} \\
&\qquad = \begin{bmatrix} c_{ij}(\mathbf{y}) & 0 & 0 \\ 0 & c(\mathbf{y}) & 0 \\ 0 & 0 & c(\mathbf{y}) \end{bmatrix}\begin{bmatrix} u_{i}(\mathbf{y},n\Delta t) \\ p^{w}(\mathbf{y},n\Delta t) \\ p^{a}(\mathbf{y},n\Delta t) \end{bmatrix},
\end{aligned} \tag{36}$$

with the integration weights, e.g.,

$$\omega^{ef}_{n}(\hat{U}^{ss}_{ij},\mathbf{y},\Delta t) = \frac{\mathcal{R}^{-n}}{L}\sum_{\ell=0}^{L-1}\int_{\Gamma}\hat{U}^{ss}_{ij}\left(\mathbf{x},\mathbf{y},\frac{\gamma(\mathcal{R}e^{i\ell\frac{2\pi}{L}})}{\Delta t}\right)N^{f}_{e}(\mathbf{x})d\Gamma e^{-in\ell\frac{2\pi}{L}} \quad . \tag{37}$$

Note that the calculation of the integration weights is only based on the Laplace transformed fundamental solutions which are available (see A.2). Therefore, with the time stepping procedure (36) a boundary element formulation for partially saturated poroelastodynamics is given without time–dependent fundamental solutions.

The numerical implementation is accomplished by using the open source C++ BEM library HyENA [32]. All regular integrations are performed with standard Gauß quadrature. The weak singular integrals are treated with a Duffy transformation. The final equation system is solved with a direct solver. Further, dimensionless variables have been introduced following the approach for the saturated case as reported in [38]. Here, the values

$$x \to \frac{x}{\kappa_w\sqrt{K\rho_w}} \qquad t \to \frac{t}{\rho_w\kappa_w} \qquad \rho \to \frac{\rho}{\rho_w} \qquad G \to \frac{G}{K}$$

have been used. This list is not complete but can be extended analogously to the not mentioned quantities like, e.g., the air density, bulk modulus, etc.

5 Numerical Examples

In this section, the previously introduced collocation boundary element method is applied on some numerical examples. At the beginning, a three dimensional partially saturated poroelastic column is calculated in time domain. The numerical results are compared with the one-dimensional (1D) semi-analytical solutions given in [26]. The sensitivity on mesh size and time

step size is investigated. Second, a partially saturated poroelastic half-space is calculated and discussed. The numerical results are analyzed and controlled by comparing with the theoretical arriving time of the fast compressional wave, the shear wave, and the Rayleigh wave. Finally, the vibration isolation of an open trench in a partially saturated poroelastic half-space is studied by using different geometry data.

For all the numerical examples, the surface is discretized with linear triangular elements. The material data of Massilon Sandstone (see table 1) are chosen. The initial water saturation is set to $S_w = 0.9$, the pore size distribution index ϑ is set to 1.5, the residual water saturation S_{rw} is set to 0, and the air entry saturation S_{ra} is set to 1. For the CQM the selected underlying multistep method is a BDF 2 (i.e., $\gamma(z) = 1.5 - 2z + 0.5z^2$) and $\mathcal{R}^N = 10^{-5}$ is applied.

5.1 A three dimensional partially saturated poroelastic column

The column has a length of 3 m and a width and height of 1 m, respectively. In order to compare with the one dimensional solution, the boundary conditions are the same as in the 1D case in [26], where no fluid flux at the bottom and around the column is allowed. The normal displacement at the bottom and the four sides is also set to zero as shown in figure 4. The top of the column

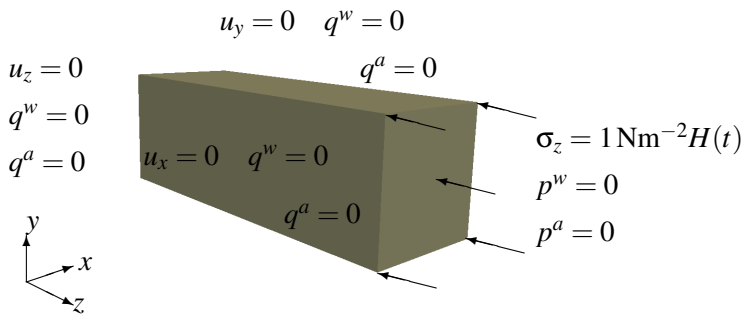

Figure 4: Geometry and boundary conditions of a three dimensional partially saturated poroelastic column

is excited by a stress jump according to a unit step function (Heaviside load). Furthermore, the Poisson's ratio is set to zero artificially.

In order to obtain good numerical results an optimal time step size Δt corresponding to the respective mesh should be chosen. As usual, this optimal choice depends basically on the wave velocities and the spatial discretization. Therefore, the dimensionless parameter

$$\beta_{CFL} = \frac{v_{p_1} \Delta t}{r_e} \tag{38}$$

is introduced, where v_{p_1} is calculated according to Gassman's equation representing the fast compressional wave velocity. The characteristic element length r_e is chosen to be the largest side of the triangle.

Three different surface meshes as shown in figure 5 with 224, 896, and 2016 linear triangular elements will be used to calculate the solid displacements and both pore pressures. The corresponding characteristic element length's r_e is $1/2$ m, $1/4$ m, and $1/6$ m, respectively.

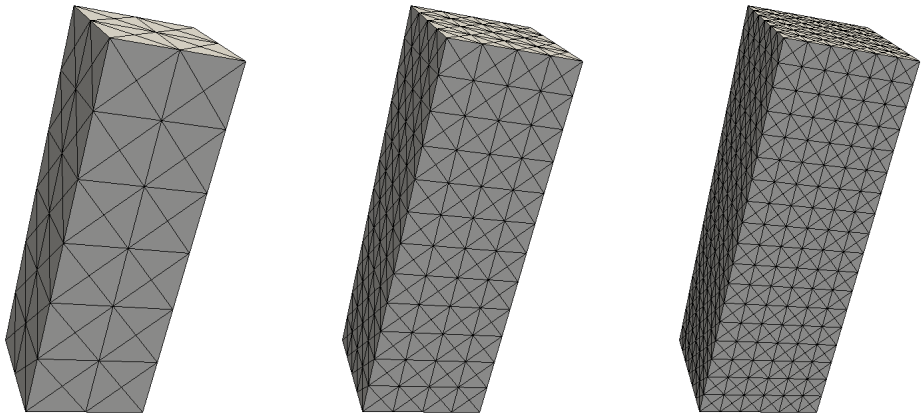

(a) $r_e = 1/2\,\mathrm{m}$ (b) $r_e = 1/4\,\mathrm{m}$ (c) $r_e = 1/6\,\mathrm{m}$

Figure 5: Different surface meshes

Influence of the spatial discretization First, the influence of the spatial discretization on the results is studied. The time domain results of the displacement and pore pressure are given in figure 6 for fixed $\beta_{CFL} = 0.3$ and varying mesh size.

The displacement results are nearly not influenced by the different mesh choices. Of course, the three dimensional numerical result coincides best with the 1D solution for the finest mesh with $r_e = 1/6\,\mathrm{m}$. The coarser meshes with $r_e = 1/2\,\mathrm{m}$ or $r_e = 1/4\,\mathrm{m}$ give good results, but show a somehow stronger numerical damping. However, the numerical results of all mesh sizes are acceptable.

On the other hand, the pore pressure results are more sensitiv on the mesh size. The best results for both the pore water and pore air pressure in comparison with the 1D solutions are obtained if the mesh size is set to $r_e = 1/6\,\mathrm{m}$. These results can be regarded as good, whereas the results of the coarser meshes $r_e = 1/2\,\mathrm{m}$ or $r_e = 1/4\,\mathrm{m}$ deviate from the analytical solution. This trend is increased for increased time. It should be remarked that the overshooting at the wave fronts in the pressure solutions can be reduced by choosing a different multistep method within the CQM [7]. But, they can not be avoided and are not related to the partial saturated porous material.

Influence of the time discretization Beside a proper mesh size, the time step is of importance in dynamic calculations since it affects the result's accuracy and the efficiency. The choice of the time step should follow the rule to be small enough for the result's accuracy and as large as possible for the calculation's efficiency. The following calculations are performed with the mesh size of $r_e = 1/6\,\mathrm{m}$ but the time step size is varied by changing $\beta_{CFL} = [0.1 \ldots 1.0]$. In figure 7, the solid displacements and the pore pressures are plotted versus time for different values of β_{CFL} in comparison with the 1D solution.

The displacement results (see figure 7a) are acceptable, no matter calculating with a large time step ($\beta_{CFL} = 1.0$, $\Delta t = 0.0001456\,\mathrm{s}$) or with a very small time step ($\beta_{CFL} = 0.1$, $\Delta t =$

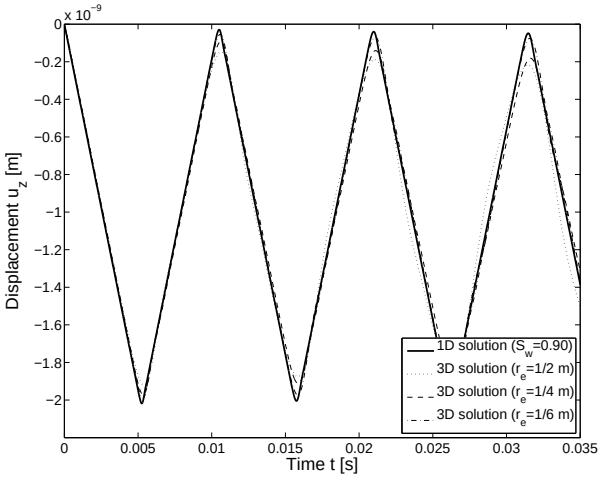

(a) Displacement u_z

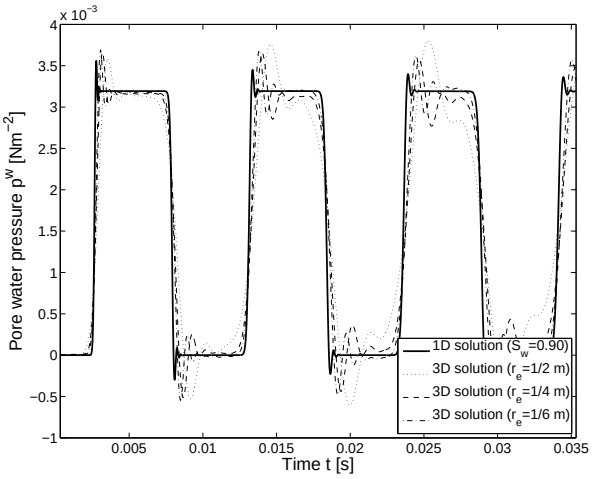

(b) Pore water pressure p^w

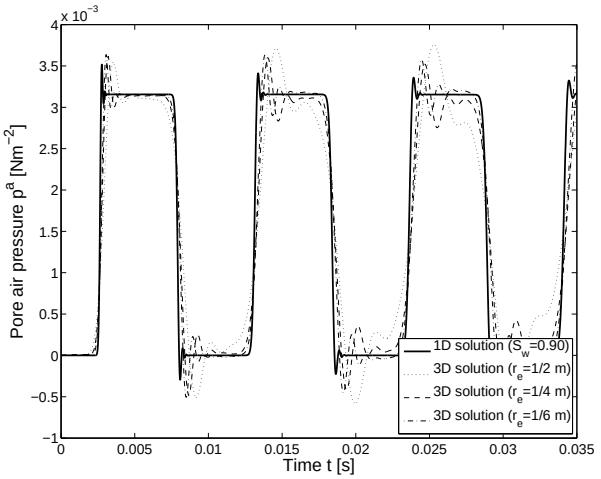

(c) Pore air pressure p^a

Figure 6: Sensitivity study on the mesh size for $\beta_{CFL} = 0.3$

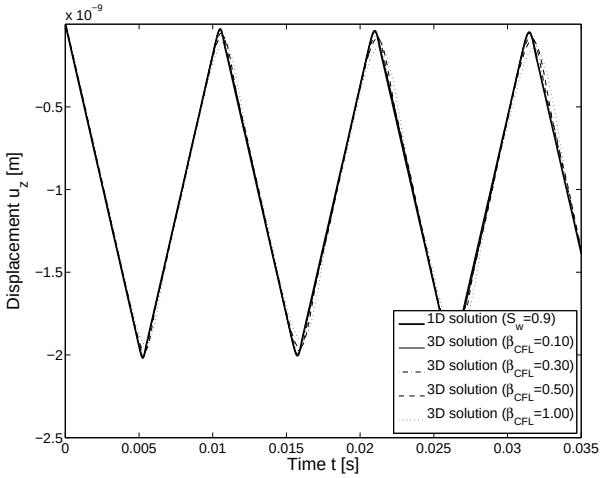

(a) Displacement u_z

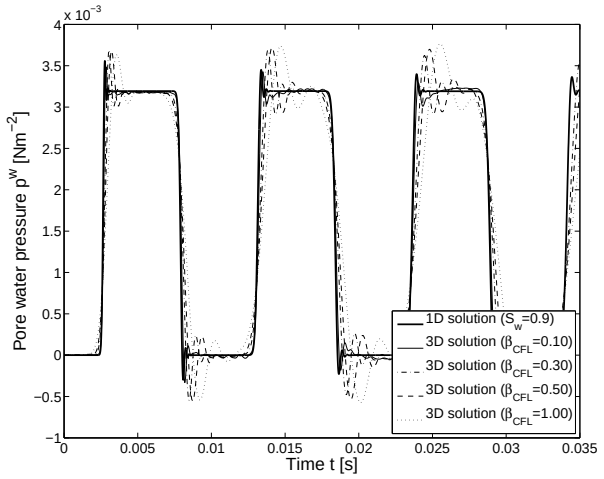

(b) Pore water pressure p^w

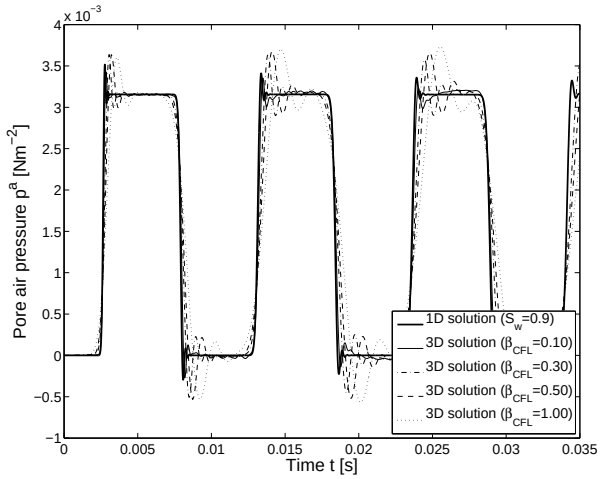

(c) Pore air pressure p^a

Figure 7: Sensitivity study on the time step size for $r_e = 1/6\,\mathrm{m}$

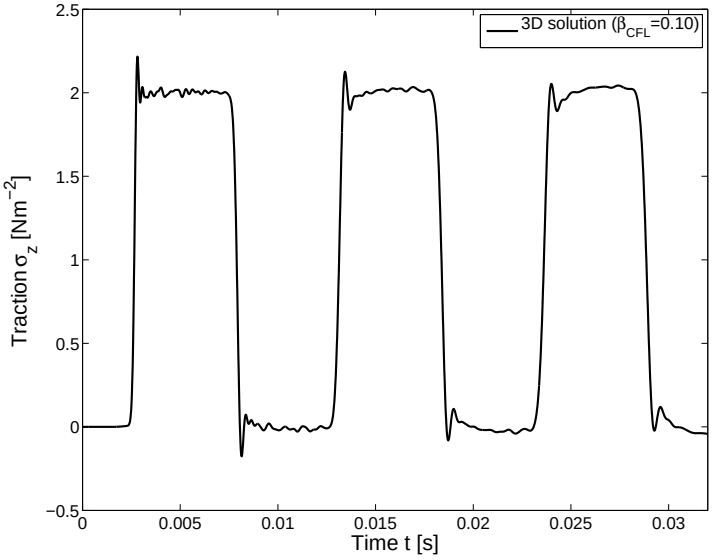

Figure 8: Traction σ_z versus time at the bottom center of the column with $\beta_{CFL} = 0.10$

0.00001456 s). The displacement results become better and better with decreasing the value of β_{CFL}, i.e., decreasing the time step size. Besides, these results show no phenomenon of instability for small time step sizes as observed in other time domain BEM formulations. This may be caused by the damping of the material, i.e., the damping caused by the friction between the solid skeletton and the flowing fluid.

The pore pressure results shown in figures 7b and 7c are acceptable and nearly independent on the time step size up to $\beta_{CFL} \leq 0.5$. For a larger time step as $\beta_{CFL} = 1.0$ the result turns worse towards a larger time period, i.e., after $t = 0.015$ s.

As already mentioned above, usually time domain BEM formulations suffer from stability problems with small time step sizes. An exception are the energy formulations (see, e.g., [2]). In standard 3D formulations mostly $\beta_{CFL} \approx 0.7$ is recommended, whereas in CQM based formulations a broader range $\beta_{CFL} > 0.1$ can be used. The above presented results do not show instabilities. However, with a very small time step size as $\beta = 0.1$ and $\Delta t = 0.00001456$ s, a slight instability can be observed for the traction result. In figure 8, fluctuations can be observed after the arrival of the fast compressional wave at $t = 0.0026$ s. After a long time period, it can be anticipated that the traction will start to blow up.

To show the differences of a partial saturated and a saturated poroelastic column, in figure 9 the displacement results are compared. All material data are the same as above, but the saturation degree is set to $S_w = 1$. The different wave speeds of a partial saturated and a full saturated poroelastic material can be clearly observed. Another difference is the absolute value of the displacements because the saturated material is more stiff than the partial saturated one. This is in accordance with the Gassmann equation [13]. In [26] this effect has been studied using the 1D solution of the above introduced model. Any effect presented there can be produced with the BEM solution and will not be repeated here.

Summarizing, the method is validated with the semi-analytical 1D solution. The displacement

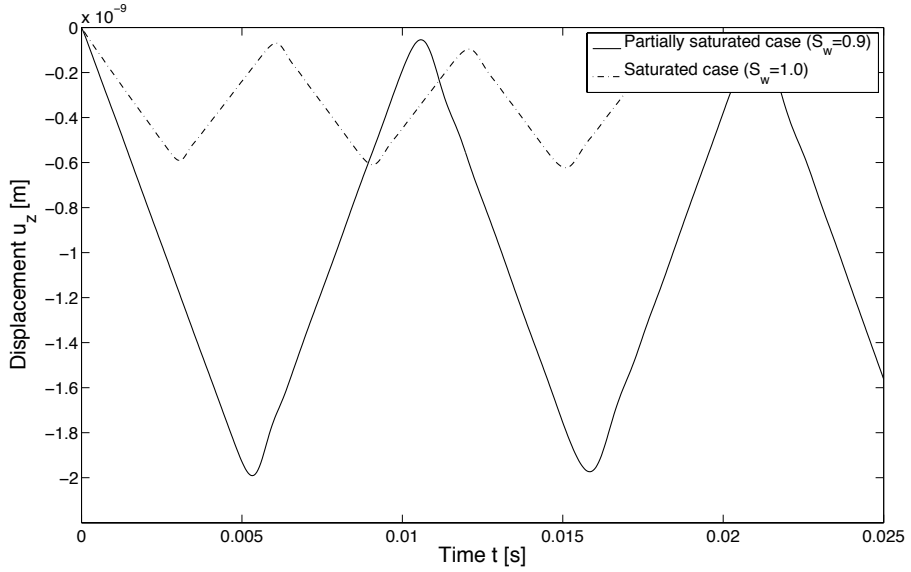

Figure 9: Comparison of the displacements at the end of the column for a saturated ($S_w = 1$) and a partial saturated ($S_w = 0.9$) model

results are much less sensitive on the mesh size than the pore pressures. The same holds for the tractions. In comparison with an elastodynamic CQM based BEM formulation a finer mesh is required to obtain the same quality of results. This is caused by the coupling of the pore pressure with the displacements. There might be an improvement if different meshes are used for displacements and pore pressures.

5.2 A partially saturated poroelastic half-space

Dealing with wave propagation in a half-space, surface waves are one of the most interesting effects. Especially, the Rayleigh wave is of interest due to the disastrous consequences in earthquakes. For elasticity, this wave velocity v_r can be approximated by the formula [18]

$$v_r = \frac{0.87 + 1.12\nu}{1+\nu} v_{p_1} \,. \tag{39}$$

This wave exists also in partial saturated porous media [3] and will be detected here. It can be expected that the overall response is similar to the elastodynamic case and the displacement result will be similar to Pekeris solution [34]. Hence, it is expected to see a damped Rayleigh pole indicating the arrival of the Rayleigh wave.

To capture this pole in a partially saturated poroelastic half-space, the proposed boundary element formulation is used. Because in the boundary element formulation applied here a full space fundamental solution is used, the free surface has to be discretized. A square surface ($5\,\mathrm{m} \times 5\,\mathrm{m}$) is discretized with two different meshes ($r_e = 1/2\,\mathrm{m}$ and $r_e = 1/4\,\mathrm{m}$, see figure 10). The modeled half-space is loaded by a vertical total stress $t_z = 1\,\mathrm{Nm}^{-2} H(t)$ on a area as shown in figure 10 and the remaining surface is traction free. Both, the pore water and pore air pressure

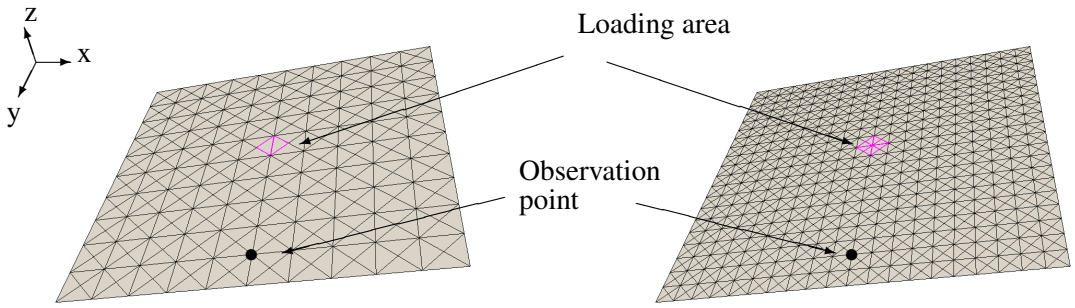

(a) $r_e = 1/2\,\mathrm{m}$ (b) $r_e = 1/4\,\mathrm{m}$

Figure 10: Different half-space surface meshes

Table 2: Wave velocities and corresponding arriving time (Laplace parameter $s = 100i$)

$V_{p_1}\,[\mathrm{ms}^{-1}]$	$V_s\,[\mathrm{ms}^{-1}]$	$V_r\,[\mathrm{ms}^{-1}]$	$t_{p_1}\,[\mathrm{s}]$	$t_s\,[\mathrm{s}]$	$t_r\,[\mathrm{s}]$
1144.76	800.55	700.68	0.00175	0.00250	0.00285

are assumed to be zero all over the surface. The observation point is located 2 m away from the loading area. The theoretical arriving times of the fast compressional wave, the shear wave, and the Rayleigh wave are computed by the equations (19b), (19d), and (39) for a fixed frequency value, respectively (see table 2). Note, the fast compressional wave and the shear wave velocities are nearly frequency independent.

When dealing with such a domain, two error sources are introduced: First, the discretization error due to the necessary truncation of the infinite boundary at some finite extent as depicted in figure 10. Second, the implication this truncation has on the definition of the integral in (33) as a Cauchy Principal Value and the regularization with partial integration. The latter requires a closed boundary. Note that this error is strictly due to the discretization, on the continuous level, where the regularization was performed, everything is correct. Overall, it can be stated that both errors are small and can be ignored.

In figure 11, the vertical solid displacement at the observation point is plotted versus time. Additionally, the arrival times of the different waves as listed in table 2 are marked with vertical dashed lines. For both meshes two different time step sizes are plotted to see the sensitivity on these parameters. The coarse mesh $r_e = 1/2\,\mathrm{m}$, independent which time step is chosen, gives very smeared in principle not sufficient results if the arrival times of the wave is in the focus of interest. On the contrary, for the finer mesh, no matter with a larger or a smaller β_{CFL}, the numerical results agree well with the theoretical arriving time of the fast compressional wave. The two slow compressional waves are not visible for the given material parameters. Due to the similar wave speeds of the shear and the Rayleigh wave, a distinction at such a short distance is not possible, which makes the identification of their arrival times nearly impossible. It is obvious that the amplitude becomes larger and the overshooting after the Rayleigh wave is smaller with

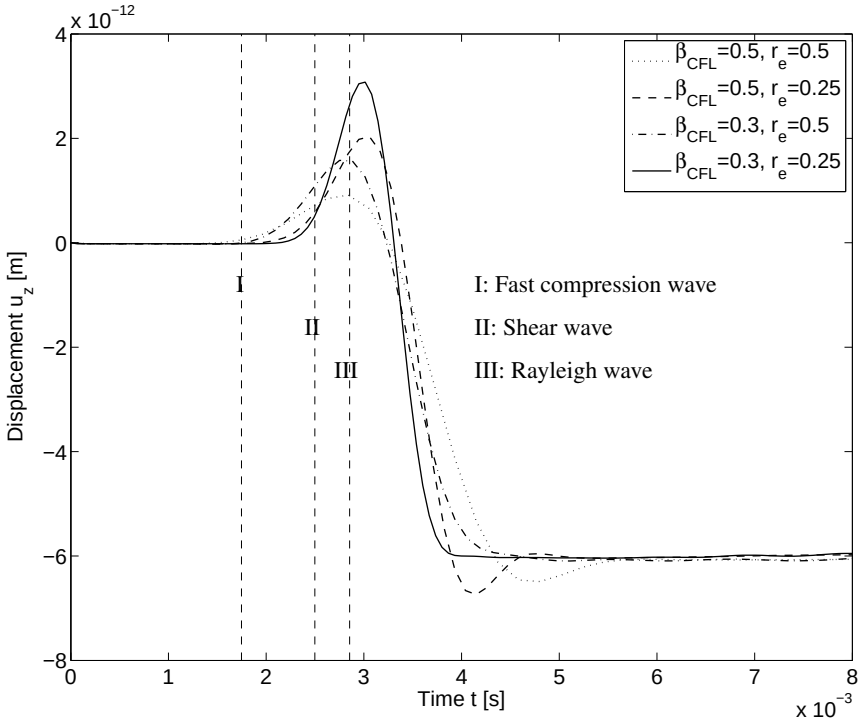

Figure 11: Vertical displacement u_z versus time

a smaller β_{CFL}. However, it must be remarked that the arrival times computed in table 2 are only valid for one frequency and, hence, in the time domain they are only an estimate. Having this in mind, it can be concluded that the results are good if the fine mesh is used, especially if the smaller time step is taken.

Next in figure 12 and 13, the displacement and the pore water pressure results below the observation point are studied. It is clearly observed that the amplitude of the Rayleigh wave peak around about $t = 0.003\,\mathrm{s}$ decreases rapidly as expected for a surface wave. For the pore water pressure, the fast compressional wave produces a pressure jump first, and with a subsequent creeping, the pore pressure drop to the final value. The pore air pressure results are not shown because they are similar to the pore water pressure.

5.3 Vibration isolation via an open trench

An interesting topic in civil engineering is vibration isolation. One possibility is the usage of trenches, which may be filled or not depending on the construction. The study of such trenches seem to be an ideal application of the BEM. Consequently, several publications in this direction exist, e.g., [23] for elastic or viscoelastic modelled soils with an shear modulus increasing with depth. Further, there are coupled FE-BE methods in frequency domain [4] or time domain [1]. Another BE approach for modeling of vibration isolation with piles can be found in [22]. Beside these numerical solutions as well analytical approaches for simply geometries of the trench has been published [21]. All the above mentioned publications assume that the soil can be modelled

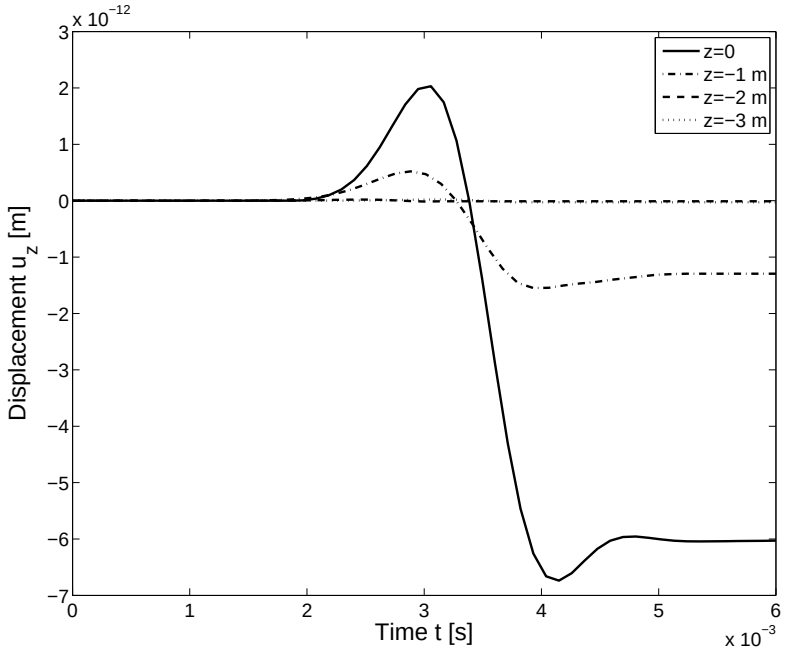

Figure 12: Vertical displacement u_z versus time below the observation point for $\beta_{CFL} = 0.5$, $r_e = 0.25$

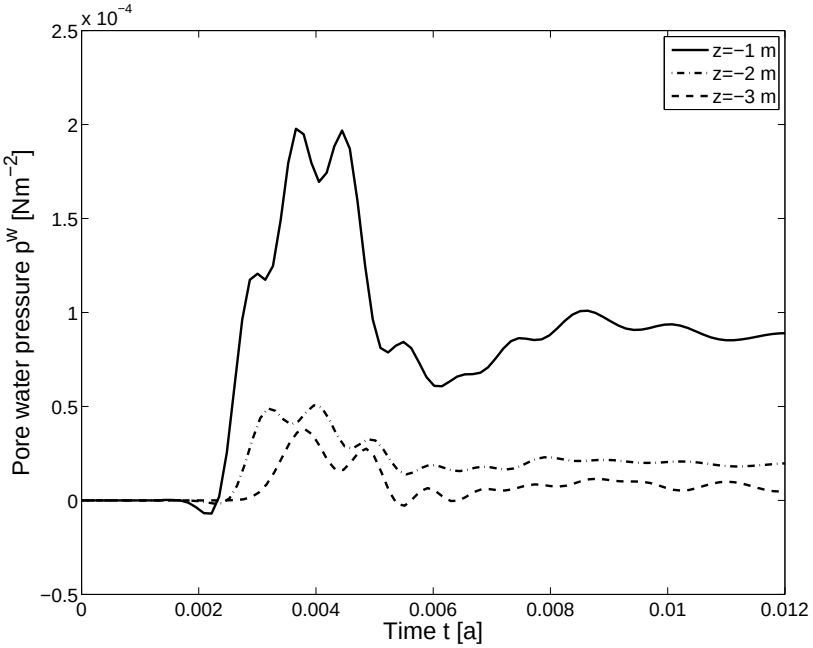

Figure 13: Pore water pressure p^w versus time below the observation point for $\beta_{CFL} = 0.5$, $r_e = 0.25$

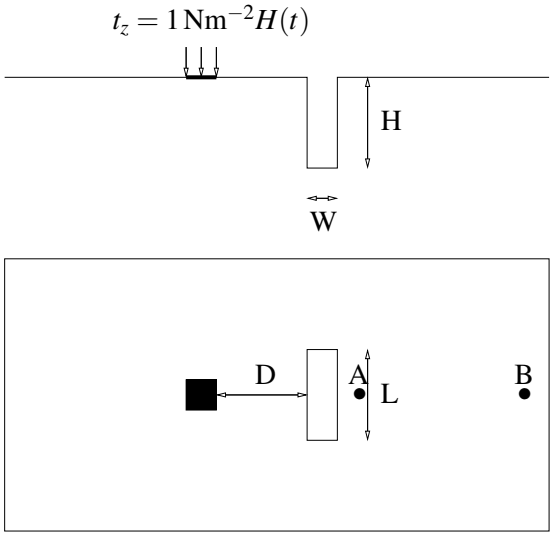

Figure 14: Geometry of the source isolation with an open trench

Table 3: Geometry parameters

		D	L	W	H
Case 1	No trench	-	-	-	-
Case 2	Shallow open trench	1.0 m	1.0 m	0.5 m	1.0 m
Case 3	Deep open trench	1.0 m	1.0 m	0.5 m	3.0 m

with a one-phase material. However, the extension of the analytical solution in [21] to saturated poroelasticity has been presented recently by Cao and Cai [10] .

Here, the vibration isolation by an open trench is studied with the proposed BEM code for the partial saturated material law. A Heaviside load is applied on the half-space where a trench with different depths is installed. A principal sketch of the problem can be found in figure 14. For the study different geometric parameters of the trench as shown in table 3 will be used. A square surface ($10\,\mathrm{m} \times 10\,\mathrm{m}$) is discretized with $r_e = 0.25\,\mathrm{m}$ (see figure 15). In the loading area a vertical total stress $t_z = 1\,\mathrm{Nm}^{-2}H(t)$ is applied and the remaining surface is traction free. Both, the pore water and the pore air pressure are assumed to be zero all over the surface. The observation points A and B (see figure 14) are 0.25 m and 4.25 m behind the trench along the center line of the trench.

Both, the vertical and horizontal responses can be a nuisance to people, sensitive laboratories, and structures. For an easy comparison of the effects of the trench, the absolute value of the displacement amplitude A_a is defined by

$$A_a = \sqrt{(u_{z_{max}} - u_{z_{min}})^2 + (u_{x_{max}} - u_{x_{min}})^2} \tag{40}$$

where $u_{z_{max}}$ and $u_{z_{min}}$ denote the maximum and the minimum vertical displacement of the observation point. $u_{x_{max}}$ and $u_{x_{min}}$ represent the maximum and minimum horizontal displacement of

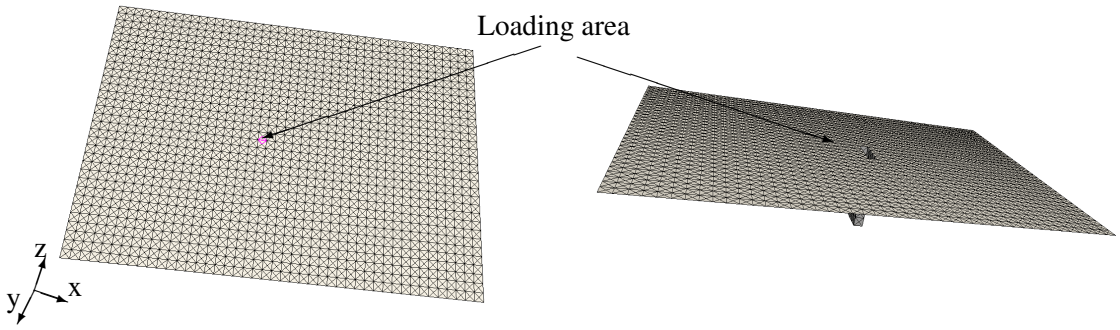

(a) $r_e = 1/4\,\mathrm{m}$, without trench (b) $r_e = 1/4\,\mathrm{m}$, with a trench ($H = 1\,\mathrm{m}/3\,\mathrm{m}$)

Figure 15: Different surface meshes of the half-space

the observation point. Since all the observation points are located in the center line of the trench u_y is zero.

In the following, the amplitude A_a is computed for each node in a line perpendicular to the trench, starting at the center to a distance of 4.5 m. The points A and B are on this line. These values are plotted versus distance in figure 16a for the cases 1 - 3 (see table 3 for the partial saturated material ($S_w = 0.9$) and for the saturated material ($S_w = 1$). Further, a reduction factor A_{rf} for the amplitudes is defined by dividing A_a by the corresponding absolute displacement value without a trench (case 1). This is presented in figure 16b. In both figures, the improvement by the trench is visible. At the point A, the absolute value of the displacement amplitude A_a can drop from $3.5 \times 10^{-12}\,\mathrm{m}$ to $2.5 \times 10^{-12}\,\mathrm{m}$ with the deep open trench, and the amplitude reduction factors of the shallow and deep open trenches are about 1.30 and 1.42, respectively. At the point B, the absolute value of the displacement amplitude can drop from $1.75 \times 10^{-12}\,\mathrm{m}$ to $1.55 \times 10^{-12}\,\mathrm{m}$ with the deep open trench, and the amplitude reduction factors of the shallow and deep open trenches are about 1.155 and 1.16, respectively. The comparison of the saturated and the unsaturated model shows that the absolut values of the displacements are smaller, which is accordance with the column solution. The explanation is the same because the saturated material is more stiff. The amplitude reduction is only influenced by the saturation degree if points close to the trench are observed and, especially, for the shallow trench.

To observe wave propagation around the trench, the displacements at some points below the surface are calculated. These points are located in a $x-z$ plane at $y = 0$. In figure 17, the values of the vertical and the horizontal displacements are shown at the times $t \approx 0.0022\,\mathrm{s}$, $t \approx 0.0031\,\mathrm{s}$, and $t \approx 0.0041\,\mathrm{s}$. Before the arrival of the fast compressional wave at the bottom of the open trench the wave is nearly blocked, i.e., behind the trench the spread of the wave is hardly to see. Afterwards, the wave behind the trench can be observed at $t \approx 0.0031\,\mathrm{s}$ and $t \approx 0.0041\,\mathrm{s}$.

A short conclusion for the vibration isolation with an open trench is that a deeper trench will produce a better isolation effect since the traveling distance of the wave will be longer. However, taking the soil as an example, a deeper trench means a more difficult maintaining work of the trench to keep the stability of the excavation and to avoid later back filling. A shallow trench but close enough to the object may be a viable solution.

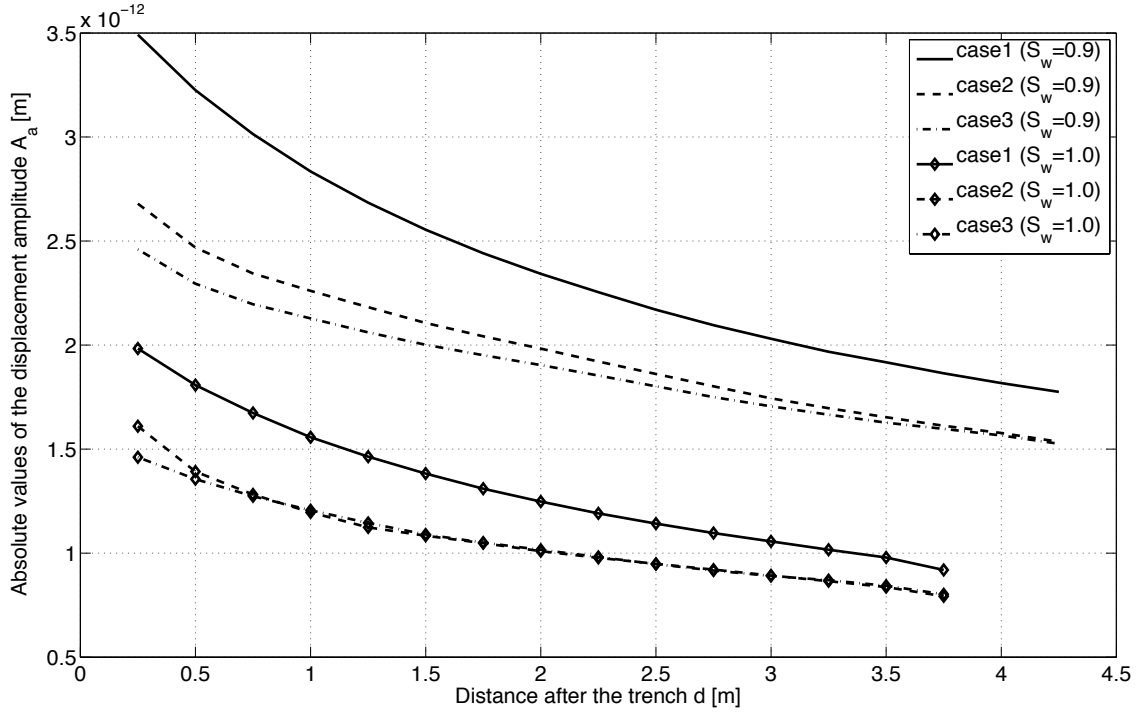

(a) Amplitude

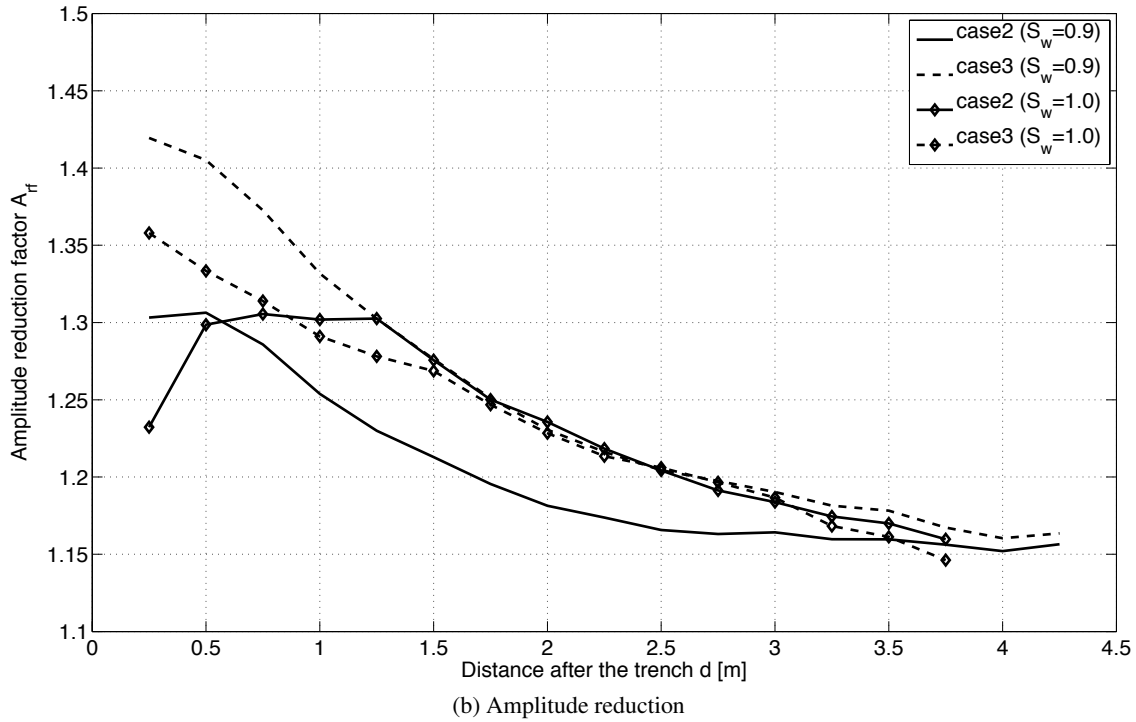

(b) Amplitude reduction

Figure 16: Displacement amplitude A_a and the corresponding amplitude reduction factor A_{rf} versus the distance behind the trench for a saturated ($S_w = 1$) and a partial saturated ($S_w = 0.9$) model

(a) u_z at $t \approx 0.0022\,\mathrm{s}$

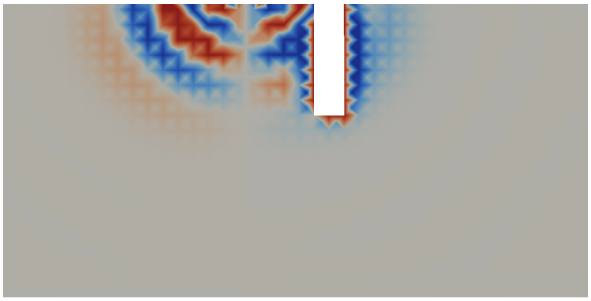

(b) u_x at $t \approx 0.0022\,\mathrm{s}$

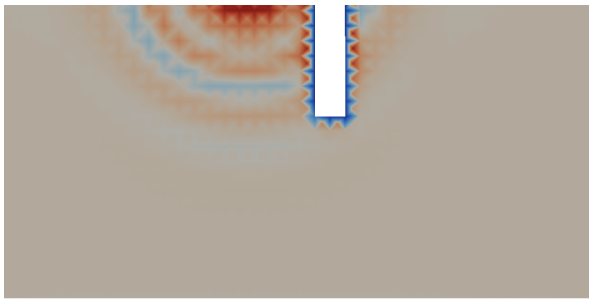

(c) u_z at $t \approx 0.0031\,\mathrm{s}$

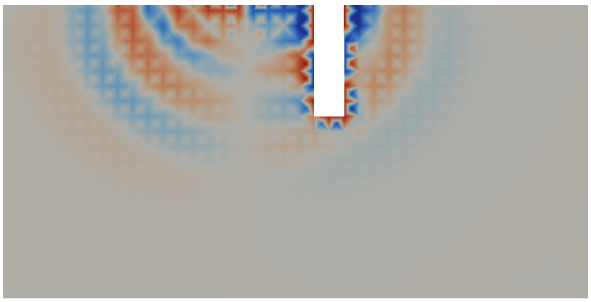

(d) u_x at $t \approx 0.0031\,\mathrm{s}$

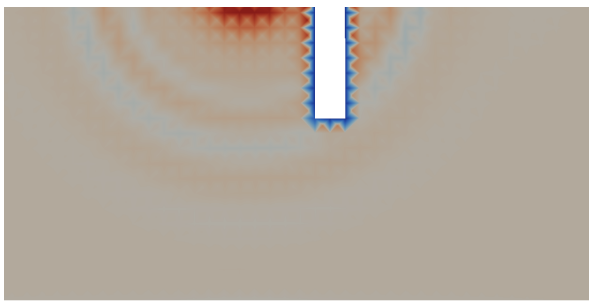

(e) u_z at $t \approx 0.0041\,\mathrm{s}$

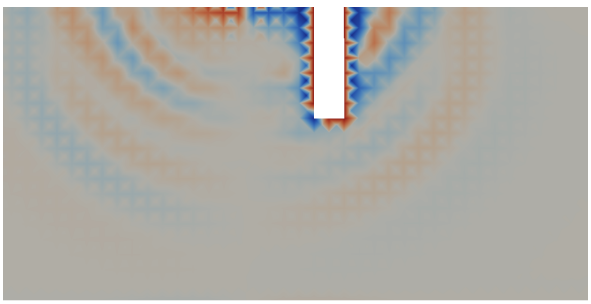

(f) u_x at $t \approx 0.0041\,\mathrm{s}$

Figure 17: Vertical (left) and the horizontal (right) displacement distribution below the surface

6 Conclusion

A collocation boundary element method has been established for partially saturated poroelasticity in 3D. The material model consists of three phases, the elastic solid phase, the wetting fluid, and the non–wetting fluid. The governing equations are derived based on the principles of continuum mechanics and the mixture theory. Aiming at a Convolution Quadrature Method (CQM) based BEM it is sufficient to state the governing equations in Laplace domain, which allows to have the solid displacements and both pore pressures as unknowns.

The fundamental solutions are derived using the method of Hörmander. The boundary integral equations can be found with a weighted residual statement. As the singularities in the fundamental solutions are similar to the saturated case, the regularization can be performed analogously, i.e., partial integration is used to obtain a weakly singular integral equation. After spatial discretisation and using the CQM as time discretisation a time stepping boundary element formulation is obtained for partial saturated media.

Three numerical examples are presented with the proposed boundary element formulation. First of all, the code is validated by calculating a three dimensional partially saturated poroelastic column and comparing it with an one dimensional semi-analytical solution. Two numerical parameters, the time step size and the mesh size are studied. The stability of the results is good and seems to better as in the saturated case. A partially saturated poroelastic half-space is also studied for investigating the fast compressional wave, the shear wave, and the Rayleigh wave. An open trench is modeled in a half-space with an impulse load. The displacements behind the trench at different observation points are calculated as well as the amplitude.

Summarizing, it can be stated that the method works, however, the storage and CPU-time demand is very high compared to the FEM. However, this drawback can be reduced by applying so-called fast methods (e.g., Adaptive Cross Approximation or fast multipole methods). To apply those techniques, first, some open points regarding the robustness of the method like proper dimensionless variables or efficient pre-conditioners has to be solved.

Acknowledgement The authors gratefully acknowledge the financial support by the Austrian Science Fund (FWF, grant No P24800-N26).

A Appendix

A.1 Abreviations

Abreviations for the governing equations and the fundamental solutions.

$$A_1 = G\nabla^2 - (\rho - \beta S_w \rho_w - \gamma S_a \rho_a)s^2 \quad ,$$

$$A_2 = K + \frac{G}{3} \quad ,$$

$$A_3 = -(\alpha - \beta)S_w \quad ,$$

$$A_4 = -(\alpha - \gamma)S_a \quad ,$$

$$A_5 = -(\alpha - \beta)S_w s \quad ,$$

$$A_6 = -(\zeta S_{ww} S_w + \frac{n}{K_w} S_w - S_u)s + \frac{\beta S_w}{\rho_w s}\nabla^2 \quad ,$$

$$A_7 = -(\zeta S_{aa} S_w + S_u)s \quad ,$$

$$A_8 = -(\alpha - \gamma) S_a s \quad ,$$

$$A_9 = -(\zeta S_{ww} S_a + S_u)s \quad ,$$

$$A_{10} = -(\zeta S_{aa} S_a + \frac{n}{K_a} S_a - S_u)s + \frac{\gamma S_a}{\rho_a s}\nabla^2 \quad ,$$

$$D_1 = -s^2 \left[\frac{a_6}{a_7} + \frac{a_{10}}{a_{11}} + \frac{a_2}{a_1 + a_3} + \frac{a_4^2 a_{11} + a_5^2 a_7}{(a_1 + a_3) a_7 a_{11}} \right] \quad ,$$

$$D_2 = s^4 \left[\frac{a_6 a_{10} - a_8 a_9}{a_7 a_{11}} + \frac{a_2(a_6 a_{11} + a_7 a_{10}) + a_4^2 a_{10} + a_5^2 a_6 + a_4 a_5 (a_8 + a_9)}{(a_1 + a_3) a_7 a_{11}} \right] \quad ,$$

$$D_3 = s^6 \frac{a_2(a_8 a_9 - a_6 a_{10})}{(a_1 + a_3) a_7 a_{11}} \quad ,$$

$$X_1 = r_1 \nabla^6 + r_2 \nabla^4 + r_3 \nabla^2 + r_4 \quad ,$$

$$X_2 = r_5 \nabla^4 + r_6 \nabla^2 + r_7 \quad ,$$

$$X_3 = r_8 \nabla^4 + r_9 \nabla^2 + r_{10} \quad ,$$

$$X_4 = r_{11} \nabla^4 + r_{12} \nabla^2 + r_{13} \quad ,$$

$$X_5 = r_{14} \nabla^4 + r_{15} \nabla^2 + r_{16} \quad ,$$

$$X_6 = r_{17} \nabla^4 + r_{18} \nabla^2 + r_{19} \quad ,$$

$$X_7 = r_{20} \nabla^6 + r_{21} \nabla^4 + r_{22} \nabla^2 + r_{23} \quad ,$$

$$X_8 = r_{24} \nabla^4 + r_{25} \nabla^2 + r_{26} \quad ,$$

$$X_9 = r_{27} \nabla^4 + r_{28} \nabla^2 + r_{29} \quad ,$$

$$X_{10} = r_{30} \nabla^6 + r_{31} \nabla^4 + r_{32} \nabla^2 + r_{33} \quad .$$

$$a_1 = G \quad ,$$

$$a_2 = \rho - \beta S_w \rho_w - \gamma S_a \rho_a \quad ,$$

$$a_3 = K + \frac{G}{3} \quad ,$$

$$a_4 = (\alpha - \beta) S_w \quad ,$$

$$a_5 = (\alpha - \gamma) S_a \quad ,$$

$$a_6 = \zeta S_{ww} S_w + \frac{n}{K_w} S_w - S_u \quad ,$$

$$a_7 = \frac{\beta S_w}{\rho_w} \quad ,$$

$$a_8 = \zeta S_{aa} S_w + S_u \quad ,$$

$$a_9 = \zeta S_{ww} S_a + S_u \quad ,$$
$$a_{10} = \zeta S_{aa} S_a + \frac{n}{K_a} S_a - S_u \quad ,$$
$$a_{11} = \frac{\gamma S_a}{\rho_a} \quad ,$$
$$r_1 = s^{-2}(a_1 a_7 a_{11}) \quad ,$$
$$r_2 = -(a_1 a_7 a_{10} + a_1 a_6 a_{11} + a_2 a_7 a_{11}) \quad ,$$
$$r_3 = s^2(-a_1 a_8 a_9 + a_1 a_6 a_{10} + a_2 a_7 a_{10} + a_2 a_6 a_{11}) \quad ,$$
$$r_4 = s^4(a_2 a_8 a_9 - a_2 a_6 a_{10}) \quad ,$$
$$r_5 = s^{-2}(-a_3 a_7 a_{11}) \quad ,$$
$$r_6 = a_5^2 a_7 + a_3 a_7 a_{10} + a_4^2 a_{11} + a_3 a_6 a_{11} \quad ,$$
$$r_7 = s^2(-a_5^2 a_6 - a_4 a_5 a_8 - a_4 a_5 a_9 + a_3 a_8 a_9 - a_4^2 a_{10} - a_3 a_6 a_{10}) \quad ,$$
$$r_8 = -a_1 a_4 a_{11} \quad ,$$
$$r_9 = s^2(a_1 a_5 a_8 + a_1 a_4 a_{10} + a_2 a_4 a_{11}) \quad ,$$
$$r_{10} = s^4(-a_2 a_5 a_8 - a_2 a_4 a_{10}) \quad ,$$
$$r_{11} = -a_1 a_5 a_7 \quad ,$$
$$r_{12} = s^2(a_1 a_5 a_6 + a_2 a_5 a_7 + a_1 a_4 a_9) \quad ,$$
$$r_{13} = s^4(-a_2 a_5 a_6 - a_2 a_4 a_9) \quad ,$$
$$r_{14} = -s^{-1} a_1 a_4 a_{11} \quad ,$$
$$r_{15} = s(a_1 a_5 a_9 + a_1 a_4 a_{10} + a_2 a_4 a_{11}) \quad ,$$
$$r_{16} = s^3(-a_2 a_5 a_9 - a_2 a_4 a_{10}) \quad ,$$
$$r_{17} = -s^{-1} a_1 a_5 a_7 \quad ,$$
$$r_{18} = s(a_1 a_5 a_6 + a_2 a_5 a_7 + a_1 a_4 a_8) \quad ,$$
$$r_{19} = s^3(-a_2 a_5 a_6 - a_2 a_4 a_8) \quad ,$$
$$r_{20} = s^{-1} a_1 a_{11}(a_1 + a_3) \quad ,$$
$$r_{21} = s(-a_1 a_5^2 - a_1^2 a_{10} - a_1 a_3 a_{10} - 2a_1 a_2 a_{11} - a_2 a_3 a_{11}) \quad ,$$
$$r_{22} = s^3(a_2 a_5^2 + 2a_1 a_2 a_{10} + a_2 a_3 a_{10} + a_2^2 a_{11}) \quad ,$$
$$r_{23} = s^5(-a_2^2 a_{10}) \quad ,$$
$$r_{24} = s(a_1 a_4 a_5 - a_1^2 a_9 - a_1 a_3 a_9) \quad ,$$
$$r_{25} = s^3(-a_2 a_4 a_5 + 2a_1 a_2 a_9 + a_2 a_3 a_9) \quad ,$$
$$r_{26} = s^5(-a_2^2 a_9) \quad ,$$
$$r_{27} = s(a_1 a_4 a_5 - a_1^2 a_8 - a_1 a_3 a_8) \quad ,$$

$$r_{28} = s^3(-a_2a_4a_5 + 2a_1a_2a_8 + a_2a_3a_8) \quad ,$$
$$r_{29} = s^5(-a_2^2a_8) \quad ,$$
$$r_{30} = s^{-1}a_1a_7(a_1 + a_3) \quad ,$$
$$r_{31} = s(-a_1a_4^2 - a_1^2a_6 - a_1a_3a_6 - 2a_1a_2a_7 - a_2a_3a_7) \quad ,$$
$$r_{32} = s^3(a_2a_4^2 + 2a_1a_2a_6 + a_2a_3a_6 + a_2^2a_7) \quad ,$$
$$r_{33} = s^5(-a_2^2a_6) \quad .$$

A.2 Partially Saturated Poroelastic Fundamental Solutions

The explicit expressions of the partially saturated poroelastodynamic fundamental solutions for the unknowns solid displacement and pore pressure are

$$\hat{U}_{ij}^{ss} = \frac{w_0}{4\pi r^3}\sum_{m=1}^{4} w_m\left[r_{,i}r_{,j}R_m(\lambda_m^2r^2 + 3\lambda_m r + 3) + \delta_{ij}(S_m r^2 - R_m\lambda_m r - R_m)\right] \tag{41a}$$

$$\hat{P}_{j}^{sw} = -\frac{w_0 r_{,j}}{4\pi r^2}\sum_{m=1}^{4} w_m(\lambda_m^4 r_{14} + \lambda_m^2 r_{15} + r_{16})(1 + \lambda_m r) \tag{41b}$$

$$\hat{P}_{j}^{sa} = -\frac{w_0 r_{,j}}{4\pi r^2}\sum_{m=1}^{4} w_m(\lambda_m^4 r_{17} + \lambda_m^2 r_{18} + r_{19})(1 + \lambda_m r) \tag{41c}$$

$$\hat{U}_{i}^{ws} = -\frac{w_0 r_{,i}}{4\pi r^2}\sum_{m=1}^{4} w_m(\lambda_m^4 r_{8} + \lambda_m^2 r_{9} + r_{10})(1 + \lambda_m r) \tag{41d}$$

$$\hat{P}^{ww} = \frac{w_0}{4\pi r}\sum_{m=1}^{4} w_m(\lambda_m^6 r_{20} + \lambda_m^4 r_{21} + \lambda_m^2 r_{22} + r_{23}) \tag{41e}$$

$$\hat{P}^{wa} = \frac{w_0}{4\pi r}\sum_{m=1}^{4} w_m(\lambda_m^4 r_{27} + \lambda_m^2 r_{28} + r_{29}) \tag{41f}$$

$$\hat{U}_{i}^{as} = -\frac{w_0 r_{,i}}{4\pi r^2}\sum_{m=1}^{4} w_m(\lambda_m^4 r_{11} + \lambda_m^2 r_{12} + r_{13})(1 + \lambda_m r) \tag{41g}$$

$$\hat{P}^{aw} = \frac{w_0}{4\pi r}\sum_{m=1}^{4} w_m(\lambda_m^4 r_{24} + \lambda_m^2 r_{25} + r_{26}) \tag{41h}$$

$$\hat{P}^{aa} = \frac{w_0}{4\pi r}\sum_{m=1}^{4} w_m(\lambda_m^6 r_{30} + \lambda_m^4 r_{31} + \lambda_m^2 r_{32} + r_{33}) \quad , \tag{41i}$$

where

$$R_m = \lambda_m^4 r_5 + \lambda_m^2 r_6 + r_7 \ (m = 1,2,3,4)$$
$$S_m = \lambda_m^6(r_1 - r_5) + \lambda_m^4(r_2 - r_6) + \lambda_m^2(r_3 - r_7) + r_4 \ (m = 1,2,3,4)$$
$$w_0 = \frac{\rho_w \rho_a s^2}{G\beta\gamma S_w S_a(K + 4G/3)}$$

$$w_m = \frac{e^{-\lambda_m r}}{\prod_{j=1, j\neq m}^{4}(\lambda_m^2 - \lambda_j^2)} \quad .$$

The traction and flux fundamental solutions are

$$\hat{T}_{ij}^{ss} = \left\{ [(K - \frac{2}{3}G)\hat{U}_{kj,k}^{ss} + \alpha s(S_w \hat{P}_j^{sw} + S_a \hat{P}_j^{sa})]\delta_{il} + G(\hat{U}_{ij,l}^{ss} + \hat{U}_{lj,i}^{ss}) \right\} n_l \tag{42a}$$

$$\hat{T}_i^{ws} = \left\{ [(K - \frac{2}{3}G)\hat{U}_{k,k}^{ws} + \alpha s(S_w \hat{P}^{ww} + S_a \hat{P}^{wa})]\delta_{il} + G(\hat{U}_{i,l}^{ws} + \hat{U}_{l,i}^{ws}) \right\} n_l \tag{42b}$$

$$\hat{T}_i^{as} = \left\{ [(K - \frac{2}{3}G)\hat{U}_{k,k}^{as} + \alpha s(S_w \hat{P}^{aw} + S_a \hat{P}^{aa})]\delta_{il} + G(\hat{U}_{i,l}^{as} + \hat{U}_{l,i}^{as}) \right\} n_l \tag{42c}$$

$$\hat{Q}_j^{sw} = \frac{\beta S_w}{\rho_w s}(\hat{P}_{j,i}^{sw} - \rho_w s \hat{U}_{ji}^{ss}) n_i \tag{42d}$$

$$\hat{Q}^{ww} = \frac{\beta S_w}{\rho_w s}(\hat{P}_{,j}^{ww} - \rho_w s \hat{U}_j^{ws}) n_j \tag{42e}$$

$$\hat{Q}^{aw} = \frac{\beta S_w}{\rho_w s}(\hat{P}_{,j}^{aw} - \rho_w s \hat{U}_j^{as}) n_j \tag{42f}$$

$$\hat{Q}_j^{sa} = \frac{\gamma S_a}{\rho_a s}(\hat{P}_{j,i}^{sa} - \rho_a s \hat{U}_{ji}^{ss}) n_i \tag{42g}$$

$$\hat{Q}^{wa} = \frac{\gamma S_a}{\rho_a s}(\hat{P}_{,j}^{wa} - \rho_a s \hat{U}_j^{ws}) n_j \tag{42h}$$

$$\hat{Q}^{aa} = \frac{\gamma S_a}{\rho_a s}(\hat{P}_{,j}^{aa} - \rho_a s \hat{U}_j^{as}) n_j \quad , \tag{42i}$$

where

$$\hat{U}_{kj,k}^{ss}\delta_{il}n_l = -\frac{w_0 r_{,j} n_i}{4\pi r^2} \sum_{m=1}^{4} w_m (1 + \lambda_m r)(S_m + \lambda_m^2 R_m) \tag{43a}$$

$$\hat{U}_{k,k}^{ws}\delta_{il}n_l = \frac{w_0 n_i}{4\pi r} \sum_{m=1}^{4} w_m (\lambda_m^6 r_8 + \lambda_m^4 r_9 + \lambda_m^2 r_{10}) \tag{43b}$$

$$\hat{U}_{k,k}^{as}\delta_{il}n_l = \frac{w_0 n_i}{4\pi r} \sum_{m=1}^{4} w_m (\lambda_m^6 r_{11} + \lambda_m^4 r_{12} + \lambda_m^2 r_{13}) \tag{43c}$$

$$\begin{aligned}(\hat{U}_{ij,l}^{ss} + \hat{U}_{lj,i}^{ss})n_l = &\frac{w_0 (r_{,i} n_j + \delta_{ij} r_{,n})}{4\pi r^4} \sum_{m=1}^{4} w_m \left[2R_m(\lambda_m^2 r^2 + 3\lambda_m r + 3) - r^2(1 + \lambda_m r) S_m \right] \\ &+ \frac{w_0 r_{,j} n_i}{2\pi r^4} \sum_{m=1}^{4} w_m R_m (\lambda_m^2 r^2 + 3\lambda_m r + 3) \\ &- \frac{w_0 r_{,i} r_{,j} r_{,n}}{2\pi r^4} \sum_{m=1}^{4} w_m R_m (\lambda_m^3 r^3 + 6\lambda_m^2 r^2 + 15\lambda_m r + 15)\end{aligned} \tag{43d}$$

$$(\hat{U}^{ws}_{i,l}+\hat{U}^{ws}_{l,i})n_l = \frac{w_0 r_{,i} r_{,n}}{2\pi r^3}\sum_{m=1}^{4} w_m(\lambda_m^2 r^2+3\lambda_m r+3)(\lambda_m^4 r_8+\lambda_m^2 r_9+r_{10}) - \frac{w_0 n_i}{2\pi r^3}\sum_{m=1}^{4} w_m(1+\lambda_m r)(\lambda_m^4 r_8+\lambda_m^2 r_9+r_{10}) \tag{43e}$$

$$(\hat{U}^{as}_{i,l}+\hat{U}^{as}_{l,i})n_l = \frac{w_0 r_{,i} r_{,n}}{2\pi r^3}\sum_{m=1}^{4} w_m(\lambda_m^2 r^2+3\lambda_m r+3)(\lambda_m^4 r_{11}+\lambda_m^2 r_{12}+r_{13}) - \frac{w_0 n_i}{2\pi r^3}\sum_{m=1}^{4} w_m(1+\lambda_m r)(\lambda_m^4 r_{11}+\lambda_m^2 r_{12}+r_{13}) \tag{43f}$$

$$\hat{P}^{sw}_{j,i} n_i = \frac{w_0 r_{,j} r_{,n}}{4\pi r^3}\sum_{m=1}^{4} w_m(\lambda_m^2 r^2+3\lambda_m r+3)(\lambda_m^4 r_{14}+\lambda_m^2 r_{15}+r_{16}) - \frac{w_0 n_{,j}}{4\pi r^3}\sum_{m=1}^{4} w_m(1+\lambda_m r)(\lambda_m^4 r_{14}+\lambda_m^2 r_{15}+r_{16}) \tag{43g}$$

$$\hat{P}^{sa}_{j,i} n_i = \frac{w_0 r_{,j} r_{,n}}{4\pi r^3}\sum_{m=1}^{4} w_m(\lambda_m^2 r^2+3\lambda_m r+3)(\lambda_m^4 r_{17}+\lambda_m^2 r_{18}+r_{19}) - \frac{w_0 n_{,j}}{4\pi r^3}\sum_{m=1}^{4} w_m(1+\lambda_m r)(\lambda_m^4 r_{17}+\lambda_m^2 r_{18}+r_{19}) \tag{43h}$$

$$\hat{P}^{wa}_{,j} n_j = -\frac{w_0 r_{,n}}{4\pi r^2}\sum_{m=1}^{4} w_m(1+\lambda_m r)(\lambda_m^4 r_{27}+\lambda_m^2 r_{28}+r_{29}) \tag{43i}$$

$$\hat{P}^{aw}_{,j} n_j = -\frac{w_0 r_{,n}}{4\pi r^2}\sum_{m=1}^{4} w_m(1+\lambda_m r)(\lambda_m^4 r_{24}+\lambda_m^2 r_{25}+r_{26}) \tag{43j}$$

$$\hat{P}^{ww}_{,j} n_j = -\frac{w_0 r_{,n}}{4\pi r^2}\sum_{m=1}^{4} w_m(1+\lambda_m r)(\lambda_m^6 r_{20}+\lambda_m^4 r_{21}+\lambda_m^2 r_{22}+r_{23}) \tag{43k}$$

$$\hat{P}^{aa}_{,j} n_j = -\frac{w_0 r_{,n}}{4\pi r^2}\sum_{m=1}^{4} w_m(1+\lambda_m r)(\lambda_m^6 r_{30}+\lambda_m^4 r_{31}+\lambda_m^2 r_{32}+r_{33}) \quad . \tag{43l}$$

References

[1] M. Adam and O. v. Estorff. Reduction of train-induced building vibrations by using open and filled trenches. *Comput. Struct.*, 83(1):11–24, 2005.

[2] A. Aimi, M. Diligenti, C. Guardasoni, I. Mazzieri, and S. Panizzi. An energy approach to space-time Galerkin BEM for wave propagation problems. *Int. J. Numer. Methods Eng.*, 80(9):1196–1240, 2008.

[3] B. Albers. Analysis of the propagation of sound waves in partially saturated soils by means of a macroscopic linear poroelastic model. *Transp. Porous. Med.*, 80(1), 2009.

[4] L. Andersen and S. R. K. Nielsen. Reduction of ground vibration by means of barriers or soil improvement along a railway track. *Soil Dyn. Earthq. Eng.*, 25(7–10):701–716, 2005.

[5] I. Ashayeri, M. K. Jafari, and M. Kamalian. Transient boundary integral equation of dynamic unsaturated poroelastic media. In D. Zeng, M . T. Manzari, and D. R. Hiltunen, editors, *Geotechnical Earthquake Engineering and Soil Dynamics IV*, chapter 121, pages 1–12. American Society of Civil Engineers, 2008.

[6] I. Ashayeri, M. Kamalian, M. K. Jafari, and B. Gatmiri. Analytical 3d transient elastodynamic fundamental solution of unsaturated soils. *Int. J. Numer. Anal. Methods Geomech.*, 35:1801–1829, 2010.

[7] L. Banjai, M. Messner, and M. Schanz. Runge-Kutta convolution quadrature for the boundary element method. *Comput. Methods Appl. Mech. Engrg.*, 245–246:90–101, 2012.

[8] A. W. Bishop and G. E. Blight. Some aspects of effective stress in saturated and partly saturated soils. *Geotechnique*, 13:177–197, 1963.

[9] R. H. Brooks and A. T. Corey. Hydraulic properties of porous media. In *Hydraulic Papers*. Colorado State Univ., 1964.

[10] Z. Cao and Y. Cai. Isolation of train-induced ground-borne vibration by trenches on a poroelastic half-space. *J. Engrg. Mech., ASCE*, 139(5):580–593, 2013.

[11] A. H.-D. Cheng, H. Antes, and N. Ortner. Fundamental solutions of products of helmholtz and polyharmonic operators. *Eng. Anal. Bound. Elem.*, 14:187–191, 1994.

[12] O. Coussy. *Poromechanics*. John Wiley & Sons, Chichester, 2004.

[13] F. Gassmann. Über die Elastizität poröser Medien. *Viertel. Naturforsch. Ges. Zürich*, 96 (1):1–23, 1951.

[14] B. Gatmiri and E. Jabbari. Time-domain Green's functions for unsaturated soils. Part I: Two-dimensional solution. *Int. J. Solids Struct*, 42:5971–5990, 2005.

[15] B. Gatmiri and E. Jabbari. Time-domain Green's functions for unsaturated soils. Part II: Three-dimensional solution. *Int. J. Solids Struct*, 42:5991–6002, 2005.

[16] B. Gatmiri, P. Delage, and M. Cerrolaza. UDAM: A powerful finite element software for the analysis of unsaturated porous media. *Adv. Eng. Softw.*, 29(1):29–43, 1998.

[17] B. Gatmiri, P. Maghoul, and D. Duhamel. Two–dimensional transient thermo–hydro–mechanical fundamental solutions of multiphase porous media in frequency and time domains. *Int. J. Solids Struct*, 47:595–610, 2009.

[18] K. F. Graff. *Wave Motion in Elastic Solids*. Oxford University Press, 1975.

[19] W. Hackbusch. *Integralgleichungen*. Teubner, 1989.

[20] H. Hörmander. *Linear Partial Differential Operators*. Springer–Verlag, 1963.

[21] A. Karlström and A. Boström. Efficiency of trenches along railways for trains moving at sub- or supersonic speeds. *Soil Dyn. Earthq. Eng.*, 27(7):625–641, 2007.

[22] S.E. Kattis, D. Polyzos, and D.E. Beskos. Modelling of pile wave barriers by effective trenches and their screening effectiveness. *Soil Dyn. Earthq. Eng.*, 18(1):1–10, 1999. ISSN 0267-7261.

[23] K. L. Leung, I. G. Vardoulakis, D. E. Beskos, and J. L. Tassoulas. Vibration isolation by trenches in continuously nonhomogeneous soil by the BEM. *Soil Dyn. Earthq. Eng.*, 10 (3):172–179, 1991.

[24] R. W. Lewis and B. A. Schrefler. *The Finite Element Method in the Static and Dynamic Deformation and Consolidation of Porous Media*. John Wiley and Sons, Chichester, 1998.

[25] P. Li. *Boundary Element Method for Wave Propagation in Partially Saturated Poroelastic Continua*, volume 15 of *Computation in Engineering and Science*. Verlag der Technischen Universität Graz, 2012.

[26] P. Li and M. Schanz. Wave propagation in a 1–d partially saturated poroelastic column. *Geophys. J. Int.*, 184:1341–1353, 2011.

[27] C. Lubich. Convolution quadrature and discretized operational calculus. I. *Numer. Math*, 52:129–145, 1988.

[28] C. Lubich. Convolution quadrature and discretized operational calculus. II. *Numer. Math*, 52:413–425, 1988.

[29] P. Maghoul, B. Gatmiri, and D. Duhamel. Three–dimensional transient thermo–hydro–mechanical fundamental solutions of unsaturated soils. *Int. J. Numer. Anal. Methods Geomech.*, 34:297–329, 2010.

[30] P. Maghoul, B. Gatmiri, and D. Duhamel. Boundary integral formulation and two-dimensional fundamental solutions for dynamic behavior analysis of unsaturated soils. *Soil Dyn. Earthq. Eng.*, 31(11):1480–1495, 2011.

[31] M. Messner and M. Schanz. A regularized collocation boundary element method for linear poroelasticity. *Comput. Mech.*, 47:669–680, 2011.

[32] M. Messner, M. Messner, F. Rammerstorfer, and P. Urthaler. Hyperbolic and elliptic numerical analysis bem library. http://www.mech.tugraz.at/HyENA, 2010.

[33] W.F. Murphy. Acoustic measures of partial gas saturation in tight sandstones. *J. Geophys. Res.*, 89(B13), 1984.

[34] C. L. Pekeris. The seismic surface pulse. *Proc. Nat. Acad. Sci. U.S.A.*, 41:469–480, 1955.

[35] M. Schanz. Poroelastodynamics: Linear models, analytical solutions, and numerical methods. *AMR*, 62(3):030803–1–030803–15, 2009.

[36] M. Schanz. On a reformulated convolution quadrature based boundary element method. *CMES Comput. Model. Eng. Sci.*, 58(2):109–128, 2010.

[37] M. Schanz and H. Antes. A new visco- and elastodynamic time domain boundary element formulation. *Comput. Mech.*, 20(5):452–459, 1997.

[38] M. Schanz and L. Kielhorn. Dimensionaless variables in a poroelastodynamic time domain boundary element formulation. *Build. Res. J.*, 53:175–189, 2005.

[39] B. A. Schrefler. Mechanics and thermodynamics of saturated/unsaturated porous materials and quantitative solutions. *AMR*, 55(4):351–388, 2002.

[40] R. Uzuoka and R. I. Borja. Dynamics of unsaturated poroelastic solids at finite strain. *Int. J. Numer. Anal. Methods Geomech.*, 36(13):1535–1573, 2012.

[41] M. Th. van Genuchten. A closed-form equation for predicting the hydraulic conductivity of unsaturated soils. *Soil Sci. Soc. Am. J*, 44, 1980.

[42] C. Wei and K. K. Muraleetharan. A continuum theory of porous media saturated by multiple immiscible fluids: I. Linear poroelasticity. *Int. J. Engng. Sci.*, 40(16):1807–1833, 2002.

[43] C. Wei and K. K. Muraleetharan. A continuum theory of porous media saturated by multiple immiscible fluids: II. Lagrangian description and variational structure. *Int. J. Engng. Sci.*, 40(16):1835–1854, 2002.

[44] O. C. Zienkiewicz, Y. M. Xie, B. A. Schrefler, A. Ledesma, and N. Bicanic. Static and dynamic behaviour of soils: A rational approach to quantitative solutions. II. semi–saturated problems. *Proc. R. Soc. Lond. A*, 429(1877):311–321, 1990.